FABRICATION OF MnO_2/ACTIVATED CARBON ELECTRODES FOR HEAVY METAL IONS REMOVAL FROM WATER USING CAPACITIVE DEIONIZATION TECHNIQUE

by

Santi Prommajan

A Thesis Submitted in Partial Fulfillment of the Requirements for the Degree of Master of Engineering in Nanotechnology

Examination Committee: Dr. Tanujjal Bora (Chairperson)
Dr. Raffaele Ricco
Dr. Chanchana Thanachayanont

Nationality: Thai
Previous Degree: Bachelor of Engineering in Chemical Engineering
Sirindhorn International Institute of Technology, Rangsit, Thailand
Scholarship Donor: His Majesty the King's Scholarships (Thailand)

Asian Institute of Technology
School of Engineering and Technology
Thailand
July 2022

AUTHOR'S DECLARATION

I, Santi Prommajan, declare that the research work carried out for this thesis was in accordance with the regulations of the Asian Institute of Technology. The work presented in it are my own and has been generated by me as the result of my own original research, and if external sources were used, such sources have been cited. It is original and has not been submitted to any other institution to obtain another degree or qualification. This is a true copy of the thesis, including final revisions.

Date:

Name (in printed letters):

Signature:

ACKNOWLEDGMENTS

I am grateful to assistant professor Dr. Tanujjal Bora for his invaluable patience and feedback. I am also thankful to assistant professor Dr. Raffaele Ricco who generously provided knowledge and expertise. And I am thankful to Dr. Chanchana Thanachayanont for her invaluable feedbacks. Additionally, this endeavor would not be possible without the scholarship from His Majesty the King's Scholarships.

I would like to extend my thanks to my colleagues, both the master students and the PhD students, for providing such crucial advice and supports; otherwise, this work would not come to fruition. And I am eternally grateful of them for creating such a welcoming working and living environment and giving me irreplaceable memories for the past 2 years. Lastly, I would like to express my deepest appreciation for my family who have been my moral and emotional support and pulled me through this endeavor.

ABSTRACT

Due to the prevalent global water crisis, susceptibility to heavy metal pollution has become concerning for many communities. As a potential solution, the capacitive deionization (CDI) technique was proposed for its energy and material recovery over the conventional metal removal techniques. In recent works, the adsorption capability is further enhanced with the incorporation of MnO_2 into the electrodes for the CDI operation. However, this type of electrode is still limited by its complex synthesis method. In this work, a simpler alternative, cyclic voltammetry electrodeposition, was used to prepare MnO_2/activated carbon cloth electrode and the effects of the synthesis conditions on the electrode's characteristics were studied. The adsorption capabilities of the electrode in CDI operation were also investigated on various metal species – chromium, cadmium, copper, and lead – with varying operating conditions: adsorption of individual metal species with varied applied voltage and flow rate, adsorption from mixtures of multiple metal species, and adsorption under continuous multiple cycle operation. Using cyclic voltammetry for the electrodeposition, the electrode's areal capacitance increased with higher depositing scan rate and depositing cycles, reaching 134.51 mF/cm^2 at 25 mV/s scan rate and 10 cycles compared to 107.25 mF/cm^2 of the raw ACC. The MnO_2/ACC electrodes in CDI operation were able to achieve the adsorption capacity of 8.76, 6.48, 3.64, and 3.41 mg/g for Cr^{3+}, Pb^{2+}, Cu^{2+}, and Cd^{2+}, respectively. The adsorption capacity would reduce with either increased flow rate or decreased applied voltage. For the adsorption from the mixtures of multiple metal species, the adsorption capacity of each species was reduced down to 2.79, 5.26, 3.52, and 1.43 mg/g for Cr^{3+}, Pb^{2+}, Cu^{2+}, and Cd^{2+}, respectively; this is attributed to the high ion activity in the solution. Lastly, for the adsorption under multiple cycles, the adsorption capacity of each species decreased with each cycle. This is believed to be from the lower desorption rate compared to the adsorption rate, reducing the available adsorption capacity in the following cycles.

Keywords: capacitive deionization, electrodeposition, MnO_2 electrode, heavy metal removal

CONTENTS

LIST OF TABLES

LIST OF FIGURES

LIST OF ABBREVIATIONS

ACC = Activated Carbon Cloth
AV = Applied Voltage
BET = Brunauer–Emmett–Teller
CDI = Capacitive Deionization
CV = Cyclic Voltammetry
EDTA = Ethylenediaminetetraacetic acid
EPZC = Potential of Zero Change
FR = Flow Rate
PDMS = Polydimethylsiloxane
pHPZC = Point of Zero Charges
SCE = Saturated Calomel Electrode
SEM = Scanning Electron Microscope
XRD = X-ray Powder Diffraction

CHAPTER 1
INTRODUCTION

1.1 Background of the Study

Humans are at risk of exposure to heavy metals from various sources in their daily activities: agricultural runoff, industrial wastewater, components in pharmaceuticals, foods, or cosmetics, residuals in electronics, and insecticides (Vardhan et al., 2019). Although some types of heavy metal can be beneficial, when it accumulates beyond what the human body can metabolize, it can cause acute and chronic health effects that can be either fatal or have long-lasting effects. Some of the symptoms include kidney dysfunction, neurological damages to children, skin cancer, myocardial infarction, muscle wasting, and partial blindness (Baby et al., 2011; Vardhan et al., 2019).

Furthermore, scarcity of clean water resources, due to the influences of overpopulation, unplanned urbanization, industrialization, and global warming, is making the situation more complex. Countries under such conditions, such as Thailand, India, and China, are often vulnerable to water pollutions and have already suffered many recorded cases of heavy metal pollution (Phenrat et al., 2016; Yu et al., 2017; Zafar Marg & Delhi, 2011). The water crisis is predicted to worsen and reach a global scale within this century, as such; countermeasures against the accompanying heavy metal pollution are of priority to achieve early mitigation.

There are many techniques available to achieve heavy metal removal from water or wastewater. Each one has its advantages and compatibility to different conditions of the water treated. However, most of these technologies still have shortcomings that limit their effectiveness as a countermeasure to heavy metal pollution under the influence of the water crisis(Barakat, 2011; Fu & Wang, 2011; Kurniawan et al., 2006). These shortcomings are mostly due to their unsustainable operations such as the heavy reliance on chemical agents of chemical precipitation, ion exchanger, and regeneration, and the high energy consumption and process complexity in employing membrane process. Therefore, despite the effectiveness of these techniques, their heavy metal removal operations may not be

cost-efficient (the membrane process in particular) or can cause environmental damages further down the line which would then further exacerbate the water crisis.

Due to the pursuit of new alternative techniques, capacitive deionization (CDI) has received interest recently as a potential candidate(R. Chen et al., 2020). CDI has been studied as an alternative to the desalination process for its low cost and low energy consumption(Porada et al., 2013). In CDI, coulombic force is used to separate charged ions from water, where they are adsorbed and stored on the surface of two electrodes (cathode and anode). The electrodes are then regenerated by simply removing or reversing the bias voltage of the electrodes.

The regeneration condition of CDI allows for repeatable operation without frequent materials replacement or chemical agents consumption, which is an advantage over the conventional techniques. Another advantage is the potential of energy recovery during the regeneration step (Han et al., 2019; Porada et al., 2013; X. Zhao et al., 2020). And depending on the system design, operation and electrode fabrication, CDI system can be scaled to various sizes, giving its versatility.

1.2 Statement of the Problem

Currently, efforts have been made on improving the performance of CDI as an alternative to the conventional heavy metal removal techniques, while also overcoming many of its limitations. One of the major limitations of CDI is from the common material used for the electrodes, porous carbon, which has low specific capacitance and is vulnerable to surface oxidation over repeated cycles, causing the CDI to suffer from low stability and low ion adsorption capacity. These limitations are major concerns due to being direct drawbacks to the advantages of CDI.

There have been many pursuits to overcome this limitation; one of those is the use of metal oxides as electrodes. Manganese dioxide (MnO_2) has shown great potential with high specific capacitance and high ion adsorption capacity due to having ion intercalation as its adsorption mechanism while not suffering the same limitation of the porous carbon. Still, MnO_2 as an electrode also has the drawbacks of low electrical conductivity and stability. Thus, one solution is the incorporation of MnO_2 together with the porous carbon substrate

(R. Chen et al., 2020; C. Hu et al., 2015; X. Zhao et al., 2020). And in place of a more common activated carbon, which required binding material which tends to hamper electrical conductivity, alternative porous carbons which are electrically conductive with stable structure, such as activated carbon cloth, were used as a substrate instead.

Nevertheless, there have not been many studies on MnO_2/carbon composite capability in removing the various species of heavy metal, and the available ones still utilize complex or expensive fabrication procedures and materials. Thus, an investigation of the MnO_2/carbon removal capability of different species of metal ions under various conditions will be beneficial to the progress of CDI. And the use of cyclic voltammetry electrodeposition as the fabrication process, which has shown ideal capacitive electrode characteristics can greatly favor the research on the MnO_2/carbon composite as CDI electrode.

1.3 Objectives of the Study

The objective of the study is to fabricate electrodeposited MnO_2/activated carbon cloth (ACC) electrodes and investigate its performance against heavy metal ion removal from aqueous medium. The specific objectives are as follows:

1. To fabricate MnO_2/ACC composite electrode by electrodepositing MnO_2 nanoparticles on ACC surface.
2. To investigate the electrodeposition parameters such as deposition rate and number of depositing cycles on the surface morphology, MnO_2 structure, and capacitive properties of MnO_2/ACC electrode.
3. To evaluate heavy metal ion removal performance of different metal ion species, individually and collectively, using MnO_2/ACC electrodes via capacitive deionization.
4. To evaluate operating parameters: cell voltage, flow rate of solutions, and number of operating cycles on the heavy metal ion removal performance of the MnO_2/ACC electrodes.

1.4 Scope of the Study

In this study, the fabrication of MnO_2/ACC electrodes using cyclic voltammetry electrodeposition was performed while investigating the effects of the scan rates and the

number of depositing cycles on the characteristics of the electrodes and the optimal conditions to obtain the best performing electrode. Surface morphology, deposited MnO_2 structure, and specific capacitance of the electrode were characterized. The heavy metal removal performance of the fabricated MnO_2/ACC electrodes were tested by studying the ion adsorption capacity of copper (Cu^{2+}), cadmium (Cd^{2+}), lead (Pb^{2+}), and chromium (Cr^{3+}), individually and collectively, from the solution. Additionally, the effect of the operating parameters (applied voltage, flow rate, and number of operating cycles) on the performance of the CDI was evaluated.

1.5 Organizations of the Study

This thesis is divided into five chapters which are schemed as follows:

Chapter 1 is composed of the background of the study, statement of the problem, objectives, scopes, and the organization of the study.

Chapter 2 describes the literature review regarding the symptoms and effect of heavy metal on living organisms and the environment; The conventional techniques for heavy metal removal; capacitive deionization: the operating mechanism, configurations, advantages, and limitations; the electrodeposition methods of MnO_2/carbon composite electrode; and the performance of capacitive deionization for heavy metal removal.

Chapter 3 presents the methodology of the processes for the fabrication of the MnO_2/activated carbon cloth electrodes; characterization of the surface morphology, deposited MnO_2 structure, and specific capacitance of the electrode; the investigation of heavy metal removal performance of the fabricated electrodes; and the CDI performance under multiple operating cycles.

Chapter 4 consists of results of the fabrication and characterization of the MnO_2/activated carbon cloth electrodes, discussion of optimized fabrication parameters, results of heavy removal performance, and discussions of optimized operating parameters for the fabricated electrodes in capacitive deionization.

Chapter 5 summarizes the study with a conclusion, application, limitations, and future recommendations for this study.

CHAPTER 2
LITERATURE REVIEW

2.1 Vulnerability to Heavy Metal Pollution

The increasing industrialization and urbanization in developing countries have given rise to serious water scarcity issues. Water usage is predicted to grow by sixth-fold in 2050 based on the population growth without the consideration of the non-uniform distribution of both the population and water resources. The severity can worsen when the growing global warming is put into consideration(Boretti & Rosa, 2019; Tortajada & Fernandez, 2018). Water scarcity can elevate the local population's vulnerability to water pollution. One of the most concerning cases is the pollution of natural water sources with wastewater often composed of heavy metals as contaminants. Even at small concentrations in sub-ppm levels, consumption of heavy metals can cause both fatal effects and long-term issues in living organisms. Furthermore, heavy metals' non-biodegradability and solubility in water make them portable and long-lasting in the environment, prolonging the contact period (Edelstein & Ben-Hur, 2018; Vardhan et al., 2019). Many countries at risk of water pollution like Thailand, India, and China, have histories of damage from heavy metal contamination (Jain et al., 2005; Phenrat et al., 2016; Yu et al., 2017). There have been cases of people living near industrial areas exposed to heavy metals due to the usage of contaminated groundwater (Polprasert, 1982; Qiao et al., 2015; Wongsasuluk et al., 2014; Yin et al., 2015).

Up to a certain extent, heavy metals in the wastewater can be absorbed by plants and aquatic creatures. However, adsorption beyond the tolerance level can severely damage the ecological systems (Chaiyara et al., 2013; Sow et al., 2019). Additionally, this can lead to bioaccumulation of heavy metals in the human food chain through fishing and aquaculture industries from water sources connected to wastewater discharge points (Chaiyara et al., 2013; Kiatsayomphu & Chaiklieng, 2012; Sow et al., 2019; Y. Wang & Fang, 2016). Therefore, preventative measures and technologies to remove heavy metals from the wastewater are critical to stopping the potential widespread damage from heavy metal contamination in water.

2.1.1 Impacts of Heavy Metal Pollution

Humans are at risk of exposure to heavy metals from various sources in their daily activities. They can be exposed through multiple sources such as water pollution from agricultural runoff and industrial wastewater, components in consumable products of pharmaceuticals, foods, and cosmetics, or residuals in manufactured products of electronics and insecticides (Vardhan et al., 2019). These heavy metals can enter the human body via multiple routes: ingestion, inhalation, and dermal absorption. Although some types of heavy metal are beneficial to the human body, it is only at a low level of concentration within a metabolic degree. When it is not, it will accumulate in soft tissues and organs, exhibiting acute and chronic health effects. The major threats to human safety among heavy metals are lead, arsenic, cadmium, and mercury, which are commonly under strict regulations (Vardhan et al., 2019). Other heavy metals can be found as pollutants and cause harmful effects on humans.

Table 2.1

Impacts of Heavy Metal's Toxicity on Human Health

Metal Species	Acute Symptoms	Chronic Symptoms
Copper	queasiness and gastric aggravation	cognitive deterioration and liver failure
Zinc	diarrhea and liver failure	pancreatic harm and anemia
Lead	abdominal pain and kidney dysfunction	mental retardation and impaired immune system
Arsenic	diarrhea, muscle cramps, and death in extreme cases	skin cancer, pulmonary and cardiovascular diseases
Mercury	shaking, muscle wasting, partial blindness	neurological damages and speech impairment

Note. Examples of acute and chronic symptoms (Vardhan et al., 2019)

Living creatures in the environment are also at risk of heavy metals, especially in the aquatic biosphere. Aquatic creatures tend to have fast larvae and juvenile phases, and changes in the environment, including temperature, food sources, and water components, can greatly affect their growth and survivability. Thus, contamination of heavy metals in the water source, even below fatal concentration, can still severely damage the biosphere. The long-term exposure at low concentration puts stress on the growing fish, causing lowered body weight, reduced size, and impairing its ability to compete for food and water. The growth inhibition of fish larvae is distinct from heavy metals and often used as a bioindicator for its contamination (Baby et al., 2011). Heavy metals can also settle and contaminate river sediment. The creatures at the bottom can accumulate these metals due to the exposure, before being fed by larger creatures, causing biomagnification of heavy metal toxins up the food chain (Baby et al., 2011).

2.2 Conventional Heavy Metal Removal Techniques

Although heavy metal pollution poses a serious risk to humans and the environment, the source of the problem is easily distinguished. Because heavy metal at fatal concentration is commonly from the release of wastewater from the industry, heavy removal techniques can simply be incorporated into the water treatment process to stop the problem. There are many techniques available to achieve heavy metal removal from water or wastewater. For example, membrane filtration, adsorption techniques, precipitation, ion exchange, etc. Each one has its advantages and compatibility with different conditions of the water treated. However, most of these technologies still have shortcomings that limit their effectiveness as a countermeasure to the ongoing water pollution (Barakat, 2011; Fu & Wang, 2011; Kurniawan et al., 2006).

2.2.1 Chemical Precipitation

Chemical Precipitation is an inexpensive and conventional heavy removal technique used in the industry. The technique utilizes a similar phenomenon to the water softening technique to achieve heavy metal removal. It utilizes chemical precipitants to react with metal ions and form insoluble precipitates which can be separated from the wastewater via sedimentation or filtration. The removal efficiency is controlled by various parameters, such as temperature, initial concentration, pH, or ion charge. Therefore, chemical

precipitation requires pre-treatment and post-treatment to control performance and collect the separated precipitates (Vardhan et al., 2019).

Despite chemical precipitation's inexpensiveness and simplicity, it is limited by the requirement for sludge separation through sedimentation or filtering, post-treatment of toxic sludge, and its reliance on a large number of chemical agents for repeating the operation. Because the metal ions will sediment into sludge, which is hard to later separate, the technique is not suitable for material recovery of valuable heavy metals. It is also not as effective in treating water with low metal concentrations. Therefore, it is commonly adapted to be used as pre-treatment or post-treatment for other techniques instead, such as ion exchange, and chemical coagulation before membrane filtration.

2.2.2 Ion Exchange

Ion exchange is a process of exchanging metal ions in the effluents with cations or anions from the ion exchanger's resins. The technique is widely used to remove ionic contaminants at low concentrations, including metal ions, because of its efficiency, fast kinetics, and lack of sludge formation. The technique also holds an advantage for its reusability via resin regeneration with chemical agents after reaching full removal capacity. Since the removed metal ions are released in the regeneration process, ion exchange is capable of material recovery as well. However, the process is susceptible to fouling from the presence of oxidants, physical contaminants, or oily substances. In addition, the process is only practical at low ionic concentrations and the biggest drawback lies in its reliance on chemical agents to regenerate the resins and continue the process (Baruth & Gottlieb, 2005).

2.2.3 Membrane Process

The membrane process is a major contributor to the water treatment industry. It is utilized in the water treatment industry for its effectiveness and its capability to separate substances over a wide range, from dissolved organic and inorganic to solid particles and microbes. The membrane process incorporates the uses of the membrane, a physical barrier that allows the bulk water stream to pass through, the permeate stream, and retain components rejected by the membranes within another stream, called concentrate or retentate (Baruth & Bergman, 2005). Substances can be removed by a membrane through various

mechanisms, either due to size exclusion, ion charges, or interaction with the membranes themselves.

The membrane process is a widely used technique, not exclusively for heavy metal removal, but also for water treatment as a whole. Because of its removal efficiency, often time, a water treatment system is designed based on having a membrane process as the main contributor in achieving the desired treated water properties. To maximize its performance and protect the membrane, feed water needs to be conditioned by various pretreatments upstream and post-treatments are also required to stabilize the treated water within reusable, or releasable conditions. As such, it is not common for the membrane process, as a technique, to be used specifically for heavy metal removal due to both the high capital cost and operational cost that come with its incorporation.

2.2.4 Adsorption

Adsorption has always been used in water treatment, but there is a growing interest in further developing the technique due to the various potentials: simplicity, inexpensiveness, reusability, and flexibility for design and customization (Carolin et al., 2017). There have also been various researches studying adsorption capability for selective removal of specific substances, such as, nitrates and phosphates, organic components, and heavy metal ions(R. Chen et al., 2020; Choi et al., 2019; Kalfa et al., 2020). The adsorption technique operates by exposing the adsorbent to the wastewater for the metal ions to be adsorbed. Because of the simplicity of the process, there are varying designs and configurations for adsorption systems. The adsorbents are also capable of regeneration whether via heat, chemical agents, or other methods. This, however, is also a drawback of the process due to the reliance on chemical agents or energy loss during thermal regeneration.

As can be seen, the conventional techniques are commonly limited by either heavy reliance on chemical agents, high operational cost, high energy consumption, or complex system design. Despite their effectiveness in heavy metal removal, they may only be viable as short-term solutions. Since many of their drawbacks can cause environmental problems in a long run, utilizing the techniques may end up redundant due to the process becoming a secondary source of environmental problems. Thus, other options for heavy metal removal

must be pursued that can achieve effective performance but do not have the same shortcomings.

2.3 Capacitive Deionization

Capacitive deionization (CDI) has been utilized in the desalination process for its low cost and low energy consumption (Porada et al., 2013), and there are growing trends toward bringing this technology into the heavy metal removal field (R. Chen et al., 2020). In CDI, columbic force is used to separate heavy metals from wastewater. The metal ions are adsorbed and stored on the surface of the electrode, commonly activated carbon, via an electrical double layer. The regeneration of electrodes is done simply by reversing the bias voltage of the electrodes. The operation, therefore, is run purely by electricity without the consumption of any chemical agents.

One of the main proposed advantages of CDI over other techniques is its potential for energy efficiency. This is due to the fact that the energy used during the electro-sorption step can be recovered during the regeneration step (Han et al., 2019; Porada et al., 2013; X. Zhao et al., 2020). Another noteworthy advantage is the lack of chemical agent consumption giving the technique a viable countermeasure against heavy metal pollution from the growing water scarcity. And due to its simple design, system operation, and electrode fabrication, CDI can be scaled to various sizes, giving it versatility and adaptability to the present systems.

Figure 2.1

Capacitive Deionization Cell & Operating Cycle

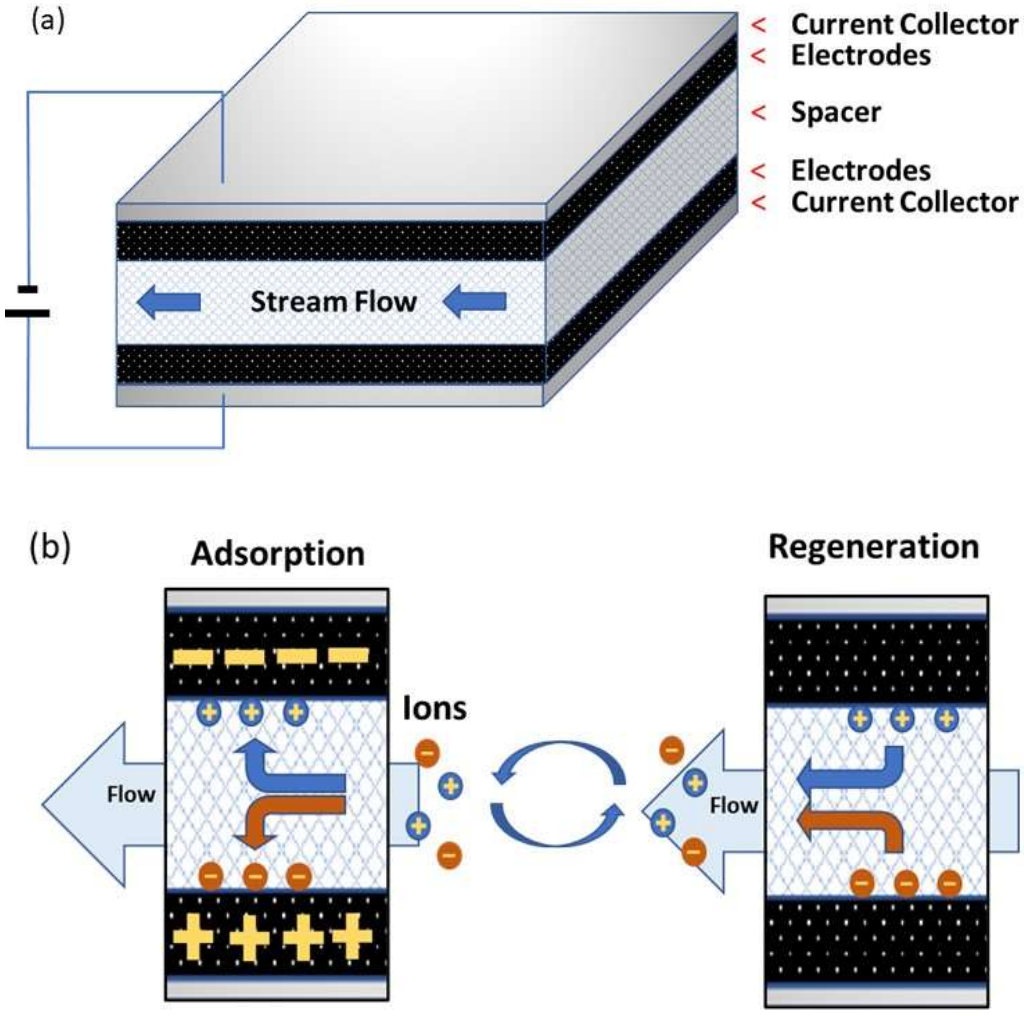

Note: These are figures of (a) CDI cell composition and (b) CDI operating cycle.

2.3.1 Working Principle

The simplest CDI cell consists of a pair of electrodes separated by a spacer channel where the feed stream flows. The electrodes are composed of current collectors for the application of voltage difference and the porous material for ion adsorption, commonly used is porous carbon. This configuration can be stacked into multiple pairs to further improve ion removal performance. A voltage difference is applied to these electrodes to attract, separate, and store the ions in the feed stream at the surface of the electrodes. When the

storage capacity is reached via saturation of the pore's surface, the electrode is regenerated by removing or reversing the voltage difference. In doing so, the ions captured will be released into the concentrated stream for further uses while the ion adsorption capacity of the electrodes is recovered (Porada et al., 2013).

2.3.1.1 **Electrical Double Layer.** The electrical double layer is the mechanism behind a conventional CDI operation. It describes the behavior of ions at the interface between a charged solid phase and the electrolyte phase. When the solid phase has excess charges, ions, mostly of opposite charges, will be absorbed and aggregated at the surface of the solid phase to compensate for the charge difference and achieve neutrality. Thus, a layer of charged solid phase and a layer of oppositely charged ions are formed, termed an electrical double layer (Anderson et al., 2010; Porada et al., 2013). Ion adsorption and storage for porous carbon electrodes are majorly contributed by the electrical double layer. Thus, most research efforts on capacitive deionization and the electrode's material are put into understanding the phenomenon and improving the ion adsorption efficiency of the electrical double layer.

However, the electrical double layer has a shortcoming in the ion adsorption performance due to the co-ion expulsion. When a potential difference is applied to the electrode, the counter ions, which have opposite charges to the electrode, are attracted and adsorbed by the electrical double layer. However, the co-ions, which have the same charges as the electrode, adsorbed on the surface or are parts of the electrode, can also be expelled back out into the stream. This is possible because both ion movements contribute to reaching charge neutrality at the electrode, and thus, co-ion expulsion could reduce the ion adsorption efficiency of the electrodes (Porada et al., 2013).

2.3.1.2 **Pseudocapacitive Ion Intercalation**. Pseudocapacitive ion intercalation is a new mechanism for CDI adsorption introduced with the new type of electrode. The mechanism occurs when the redox reaction acts as the driving force for the insertion of ions within the lattice sites of the materials, followed by electron charge transfer between the ions and the materials without changing the phase of the material (Elisadiki & King'ondu, 2020). With ion intercalation, the faradic electrodes can achieve higher ion adsorption and energy density than what the conventional electrodes can achieve with the

electrical double layer. Additionally, since the ion adsorption mechanism is different, ion intercalation does not suffer the drawback of co-ion expulsion common to the conventional capacitive deionization. However, because the redox reaction is the driving force of the process, the faradaic electrode falls short in terms of adsorption rate compared to porous carbon electrodes (Suss & Presser, 2018).

2.3.2 Materials for Electrode

Similar to the field of capacitive energy storage, the porous electrode is predominant in the CDI field, thus the popularity of porous carbon materials. This is mainly because the main phenomenon involving ion adsorption is the electrical double layer, which is enhanced by the large specific surface area found in a porous material. However, through ion intercalation and other pseudocapacitive phenomena, new alternative materials have gained interest in recent years, such as carbon polymer composite, metal oxide composite, and Mxene (a material composed of either transition metal carbide, nitride, or carbonitride formed into a thin 2D layer). And with the new adsorption mechanism, the new material may overcome certain weaknesses of the conventional materials that have limited the performance of CDI.

2.3.2.1 **Activated Carbon.** Out of all the porous carbons, activated carbon has always been among the first choices in water treatment technology for various reasons. Its low cost and high specific surface area are favorable for various applications. Moreover, due to the wide range of viable precursors, this allows for a similarly wide range of variations in structure and properties, granting flexibility for adaptation to specific applications. For CDI, it is desirable for the activated carbon to have a higher total pore volume or specific surface area due to an often direct correlation of increased ion adsorption capacity (Porada et al., 2013).

However, the challenge of using carbon electrodes is the oxidation of the anode's carbon surface over time. The accumulating oxide changes the surface charge states, including the point of zero charges (pHPZC) and potential of zero change (EPZC), which greatly reduce both performance and lifetime of the electrodes (Cohen et al., 2013). The electrode oxidation along with the co-ion expulsion due to the electrical double layer has greatly limited the performance of conventional CDI from achieving the same effectiveness as the

conventional techniques. As such, new alternative materials, and modifications to the conventional are studied to overcome these limitations.

2.3.2.2 **Metal Oxide Composite.** Due to the favorable properties of metal oxides, ranging from high hydrophilicity and alteration of the surface zeta potential, they have been incorporated with carbon material into metal oxide composite as electrodes to greatly improve the performance of CDI (B. J. Lee et al., 2007; Yanping Zhang et al., 2009). Pristine MnO_2 has been favorably used as one of the electrodes in a hybrid CDI due to its electrochemical properties, and high electrosorption capacity via ion intercalation. Its use as an anode greatly improved adsorption capacity and stability as it does not suffer from oxidation the same as a carbon electrode(Tan et al., 2020; Wu et al., 2018). However, its performance is limited by its low conductivity(Lin et al., 2018). As such, there have been pursuits of a metal oxide composite between manganese oxide and carbon electrode to overcome the drawback.

A thin film MnO_2/carbon fiber electrode was prepared via electrodeposition and tested its adsorption capability on Cu^{2+}, achieving significant specific capacitance (387 F/g) and adsorption capacity of 172.88 mg/g(C. Hu et al., 2015). Zhao et al. were able to achieve great specific capacitance and electrosorption capacity with MnO_2 decorated mesoporous carbon electrodes (C. Zhao et al., 2017). High specific capacitance(>300 F/g), stability, charge efficiency, and ion adsorption capacity (17.8 mg/g) were achieved with MnO_2/Ag coated porous carbon electrodes (Li & Park, 2018). There is also research studying its capability in the CDI system to adsorb copper from the solution (C. Hu et al., 2015). As such, the MnO_2 decorated carbon electrode may be a viable candidate for CDI electrodes suitable for heavy metal removal purposes.

However, many of the works on MnO_2 electrodes utilize complex or expensive fabrication processes that can be very limited in either scaling to factory level or mass production(Byles, Cullen, et al., 2018; Byles, Hayes-Oberst, et al., 2018; Shi et al., 2018). As such, a simpler, scalable, and inexpensive fabrication method may benefit future improvement and practical adaptation. One such option is the electrodeposition of MnO_2

instead of the usual hydrothermal method. Electrodeposition via cyclic voltammetry in particular has shown promising results with greatly improved specific capacitance.

Several works had investigated the effect of the electrodeposition method on the properties of the deposited MnO_2 (Broughton & Brett, 2005; Prasad & Miura, 2004; Shinomiya et al., 2006). And based on the work of both (Prasad & Miura, 2004; Shinomiya et al., 2006), although there is no distinct difference in capacitive behavior, the cyclic voltammetry deposition achieved higher specific capacitance compared to other deposition methods. This change in property was linked to the difference in the deposited structure of MnO_2. With cyclic voltammetry, the deposited structure was able to achieve higher mesopore density due to its smaller nanocrystal structure compared to other methods.

And in terms of the crystal structure, all deposition methods exhibited amorphous crystal structure, even after post-deposition annealing below the temperature of 500 °C. At annealing temperatures above 500 °C, the formation of crystal structure attributed to Mn_2O_3 occurred. The effect of heat treatment is further studied in several works (Chang et al., 2004; C. C. Hu & Tsou, 2002), which had found that higher annealing temperatures above 200 °C will reduce the capacitive performance in exchange for improved stability. This is concluded to be the effect of the reconstruction of the morphology at higher annealing temperatures. The drastic reduction of the capacitance is observed at the annealing temperature where the crystal structure of Mn_2O_3 formed.

The electrodeposition mechanism of MnO_2 is investigated in the work of (Dupont & Donne, 2014). During the process, the Mn^{2+} is oxidized to Mn^{3+} and then deposited into MnOOH via hydrolysis reaction. The deposition is observed from the nucleation activities of MnOOH crystallites. Afterward, the increased activity of crystal growth overshadows the nucleation, allowing for the MnOOH to transform into MnO_2 via solid-state oxidation. The transition was identified when the decrease in surface area was observed over the course of the deposition. This characteristic of the transition is also observed by several works that reported reduced surface area in electrodes prepared under longer deposition time.

2.4 Heavy Metal Removal Using CDI

CDI's application is not limited to desalination. Due to the nature of its mechanism, there is a growing trend in branching off toward new applications for CDI, such as heavy metal removal. However, as a branching application, studies in this field are still trying to catch up with its counterpart's advancement for desalination. And due to the myriad of metal species and the complexities involved in their adsorption mechanism, the research in the field is further spread out.

2.4.1 Cadmium

Activated carbon cloth was used to remove chromium in the work of (Z. Huang et al., 2016) achieving 31.85% removal efficiency in a 0.5 mM Cd^{2+} solution. Although in the presence of lead and chromium, its adsorption was greatly suppressed. It is hypothesized that charges and hydrated radius have a major effect on adsorption. And of the 3 species, chromium was adsorbed the most due to the higher charges, seconded by lead which has a smaller hydrated radius despite the same level of charges.

An activated carbon fiber electrode was modified with manganese oxide and exhibited improved adsorption of cadmium of 14.88 mg/g against 2.33 mg/g of raw AC fiber at 1.5 V (Y. Chen et al., 2015). The increased adsorption was attributed to the ion intercalation of cadmium ions by the MnO_2 deposits. Although, it still suffered under operation with high ion activity solution, a common limitation of CDI. There is also a study by (Yujie Zhang et al., 2019) of the deposited polypyrrole/chitosan electrode on adsorption of cadmium with 51.1% removal from a 1000 mg/L Cd solution at 1.5 V. The polypyrrole was utilized for its ion exchange adsorption, and the chitosan was utilized as a substrate to reinforce the electrode's stability. Many of the studies on electrodes used for cadmium adsorption focused on utilizing electrode material capable of electrochemical adsorption which has shown greater adsorption compared to porous carbon electrodes.

2.4.2 Chromium

Adsorption of Chromium has been shown to be effectively adsorbed by various types of carbon electrodes. Derivative carbon, made from biomass and agricultural waste, and commercial activated carbon were studied in Cr water treatment, showing effective

capability in removing Chromium (Gaikwad & Balomajumder, 2017; X. F. Zhang et al., 2018; Ziati et al., 2017). Other types of carbon electrodes, such as carbon aerogels (Rana-Madaria et al., 2005) and carbon nanotubes (Y.-X. Liu et al., 2011; H. Wang & Na, 2014), who benefit from their higher surface area were also investigated for chromium removal. And although they suffer from the high density of micropore or inaccessible pore structure, significant adsorption of 99% removal from a 2 mg/L Cr solution at 0.8 A·h for graphene and 96% from a 12 mg/L Cr solution at 1.4 V for CNT.

One specific property of chromium ions is the capability to form as Cr(III) cation and Cr(VI) anion. Therefore, adsorption of both forms has to be considered as they are adsorbed in opposite electrodes during operation. However, because Cr(VI) can readily reduce to Cr(III), there are also studies on the modification of the electrode which will capture Cr(VI), reduce, and release them in the less dangerous form of Cr(III) instead(Y.-X. Liu et al., 2011; H. Wang & Na, 2014).

2.4.3 Copper

Due to its common presence across the industry, many studies have been made to remove copper from the solution. For activated carbon electrodes, adsorption performance was improved by modification of the surface functional group with hydroxyl group and carboxyl and amine group, achieving 32.8 and 54.3 mg/g, respectively (Huang & Su, 2010). Additionally, improved adsorption of copper, 56.62 mg/g from a 200 mg/L Cu solution at 0.9 V was observed in ordered mesoporous carbon compared to commercial activated carbon. This was explained by the increased mesopore allowing for easier movement for copper ions. Modification of carbon substrate with metal oxide also achieves effective copper removal whether for Fe_3O_4/graphene electrode(Bharath et al., 2017) and TiO_2/reduced graphene oxide electrode(Bautista-Patacsil et al., 2020).

2.4.4 Lead

Myriad types of carbon electrodes were studied for their adsorption of lead ions. With the activated carbon electrode, it was able to achieve adsorption of 17.71 mg/g from a 5 mg/L Pb solution at 0.13 V vs. SCE, where the adsorption reaction was investigated as the binding of lead ion to a carboxylic or hydroxyl functional group (Ziati & Hazourli, 2019). For graphene electrode, it was grafted with EDTA to provide an additional adsorption

mechanism, resulting in a higher performance of 99.9% removal from a 140 mg/L Pb solution at 1.4 V (P. Liu et al., 2017). Adsorption of lead using CNT coated with stainless steel was also improved compared to normal CNT electrodes, achieving 97.2% and 99.6% in 20 mg/L and 150 mg/L Pb solution at 2 V vs. SCE (Y. Liu et al., 2013).

Many studies have shown that CDI is capable of heavy metal removal, investigating different types of electrodes and their adsorption mechanism's affinity to the metal species. There have also been ample studies of MnO_2/ACC electrodes on heavy metal removal, although mostly populated by hydrothermally prepared electrodes. Therefore, it has become one of the objectives of this thesis to investigate the performance of MnO_2/porous carbon electrodes prepared with the electrodeposition process in heavy metal removal under CDI operation.

2.5 Chapter Summary

With the growing population and industrialization, many communities become more at risk of water scarcity and more vulnerable to water pollution. One of the concerns is heavy metal pollution. Heavy metals pose fatal effects at very low concentrations and can also leave detrimental and long-lasting effects on humans and creatures in the biospheres. Although there have already been multiple conventional techniques in treating metal pollution, they are still lacking in terms of dealing with the problem in long term due to either energy consumption or creating secondary pollution.

Thus, there is growing interest in capacitive deionization as an alternative metal removal technique. This is because of its capability in attracting and adsorbing only ions from the solution. Additionally, it also has major advantages over other techniques from being an electrically driven process, making it free of chemical agent usage, and also capable of recovering energy during its desorption process. There have been efforts in introducing new electrode materials that provide additional adsorption mechanisms. One of interest is the MnO_2/ACC electrode capable of ion intercalation. Although there have been studies that have shown its capability in desalination and heavy metal removal, the material can be limited due to the complex synthesis process. Thus, it is in my interest to investigate the

capability of MnO_2/ACC prepared using electrodeposition for heavy metal removal in CDI operation.

CHAPTER 3
METHODOLOGY

3.1 Materials Used in This Study

In this study, the carbon substrate used was woven activated carbon cloth (Zorflex FM-100, USA) with a thickness of ca. 1 mm. $MnSO_4 \cdot H_2O$ (99%, Loba Chemie™, India) was used as MnO_2 precursor and Na_2SO_4 (99%, Univar™, USA) was used as a supporting electrolyte; $Na(CH_3COO) \cdot 3H_2O$ (99.5%, AR grade, Loba Chemia™, India) was used in the beginning but was changed due to formation of contaminants on the samples. HNO_3 (Nitric acid 65%, EMSURE®, Germany) was used to prepare a 5% HNO_3 for the surface activation of activated carbon cloth; KOH (KOH 85%, AR, ACI Labscan, Thailand) and HCl (fuming 37%, EMSURE®, Germany) were previously used for surface activation but was changed due to producing inconsistent sample's characteristics. The same KOH was used to control the pH of the depositing solution. Table salt was used to prepare 1000 ppm NaCl solution for the salt adsorption test. The following chemicals were used to prepare metal ion solutions: $Cu(NO_3)_2$ (99%, Univar™, USA); $Pb(NO_3)_2$ (99%, Univar™, USA); $Cd(NO_3)_2 \cdot 4H_2O$ (99%, Loba Chemie™, India); and $Cr(NO_3)_3 \cdot 9H_2O$ (98%, Himedia™, India).

3.2 Preparation of ACC Substrates

Activated carbon cloths were cut up in 2 sizes, 2x1 cm for characterization, and 3x3 cm to be used as electrodes in the CDI cell. The latter batch would be prepared after the optimal depositing condition was identified. The cut carbon cloths were first cleaned by sonication in acetone, ethanol, and DI water for 30 minutes each, then dried in the oven at 80 °C for 8 hours. The surface activation was performed on the activated carbon cloths to ensure uniform deposition on the substrate. In the beginning, KOH was used for surface activation by immersing the cloths in 1 M KOH at 80 °C for 1 hour, followed by 0.1 M HCl for 2 hours. The sample would be washed in DI water before drying in a vacuum oven at 105 °C for 24 hours. The surface activation method was changed due to producing inconsistent samples results; the results will be further discussed in chapter 4, result and discussion. The

surface activation was changed to immersion in a 5% HNO_3 aqueous solution for 30 minutes and washed with DI water.

3.3 Fabrication of the MnO_2/Activated Carbon Electrodes

The depositing solution was prepared using 0.1 M $MnSO_4 \cdot H_2O$ and 0.1 M Na_2SO_4 in DI water, acting as MnO_2 precursors and supporting electrolytes, respectively. Previously, $Na(CH_3COO) \cdot 3H_2O$ was used as supporting electrolytes but was later changed due to the formation of contaminants on samples which will be further discussed in chapter 4, result and discussion. The pH of the depositing solution was increased to 5.6 using a diluted 0.05 M KOH solution. The activated carbon cloths were immersed in the depositing solution and put under vacuum for 30 minutes to remove air bubbles and ensure uniform distribution of the solution within the pore structure. The activated carbon cloths were then moved to another depositing solution.

As shown in figure 3.1, depositions of MnO_2 were performed in a three-electrode cell setup with activated carbon cloths, 3x5 cm graphite, and an Ag/AgCl reference electrode as a working electrode, a counter electrode, and a reference electrode, respectively. The Ag/AgCl reference electrode had the potential of 196 mV against RHE and all potentials in the present study are reported against the Ag/AgCl reference electrode. Preceding the arrival of the ordered potentiostat, batches of samples were prepared using the amperometry method with a two-electrode cell setup similar to figure 3.1, exchanging the potentiostat with a power supply and without using the reference electrode. The purpose of using amperometry as an electrodeposition method was to study the viability of the lab's condition for the deposition of MnO_2 onto activated carbon cloths. After the potentiostat was shipped to the lab, the electrodeposition method was changed to cyclic voltammetry as per the objectives of the thesis.

Figure 3.1

Three Electrode Cell Setup for MnO_2 Deposition

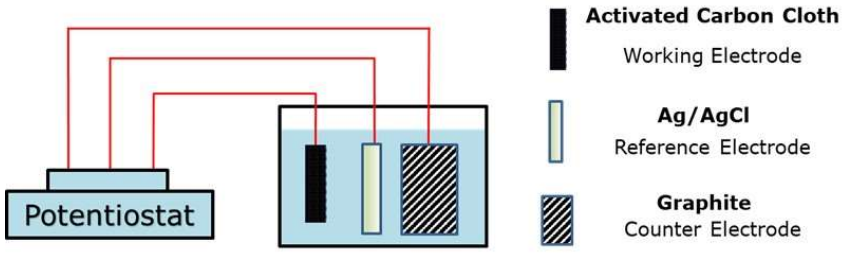

The cyclic voltammetry electrodeposition was done using a potentiostat (Ossila™ potentiostat) over the range of 0 – 1.2 V while the scan rate and deposition cycles were varied between 10, 25, and 50 mV/s and 5-10 cycles, respectively. The deposition was carried out at room temperature. Afterward, the electrodes were washed with DI water and then dried in an open-air oven for 8 hours at 80 °C. Amperometry was performed by applying fixed voltage, varied between 0.8 – 1 V, with a power supply for a duration varied between 5 – 10 minutes.

3.4 Characterization of the Fabricated Electrodes

The surface morphology of the MnO_2/ACC was examined using Field Emission Scanning Electron Microscope (FE-SEM, JEOL JSM7800F, JAPAN). The SEM was operated with the accelerating voltage of 2 kV and the magnification of 1,000-10,000. The crystal structure was examined using X-ray powder diffraction (XRD, Rigaku TTRAX III, 50kV, 300mA, Cu/K_α, 1.54059Å). The XRD results were recorded between 10°-70°(2θ) with a scan step size of 0.02°.

3.5 Electrochemical Characterization of the Fabricated Electrodes

Cyclic voltammetry was used to study capacitive behavior and calculate the specific capacitance of the fabricated electrodes. A three-electrode cell with a 0.1 M Na_2SO_4 aqueous electrolyte solution was used where a 1x2 cm^2 MnO_2/ACC sample was connected as a working electrode, the platinum wire was used as a counter electrode, and the Ag/AgCl electrode as the reference electrode. Cyclic voltammetry was performed using the

potentiostat (Ossila™ potentiostat). The voltammogram was recorded within the potential window of 0-1.0 V at multiple scan rates: 10 - 25 $mV \cdot s^{-1}$. The specific capacitances and areal capacitance from the CV curve were calculated using the following formula:

$$C_a = \frac{\int_{V_a}^{V_c} I dV}{2Av(V_c - V_a)} \qquad \ldots(3.1)$$

where C_a = Areal capacitance

I = the instant current

A = Geometric area of the electrode

v = the potential scan rate

V_c and V_a = the high and low potential limits of the CV tests

3.6 Capacitive Deionization Cell Assembly

A CDI cell was prepared by assembling the CDI layers consisting of the MnO_2/activated carbon cloth, a raw activated carbon cloth, and a filter paper. The MnO_2/activated carbon cloth and the raw activated carbon cloth acted as electrodes, and the filter paper acted as a spacer. These components were prepared to have a dimension of 3 cm x 3cm, layered in the order as shown in figure 3.2, and stacked within a hollowed squared space of a PDMS layer with a thickness of 1 mm. The layers were then sealed off between two graphite foils which also acted as current collectors; the foils were cut to have sections that can be connected to external cables. Two acrylic plates with 4 screws at each corner were used to press the CDI cell together to prevent any leakage. Two openings were made through the acrylic plates and graphite foils where plastic connectors can be inserted. The connectors would then be connected to PVC tubes for liquid flow.

Figure 3.2

Schematic Showing the Capacitive Deionization Cell Assembly

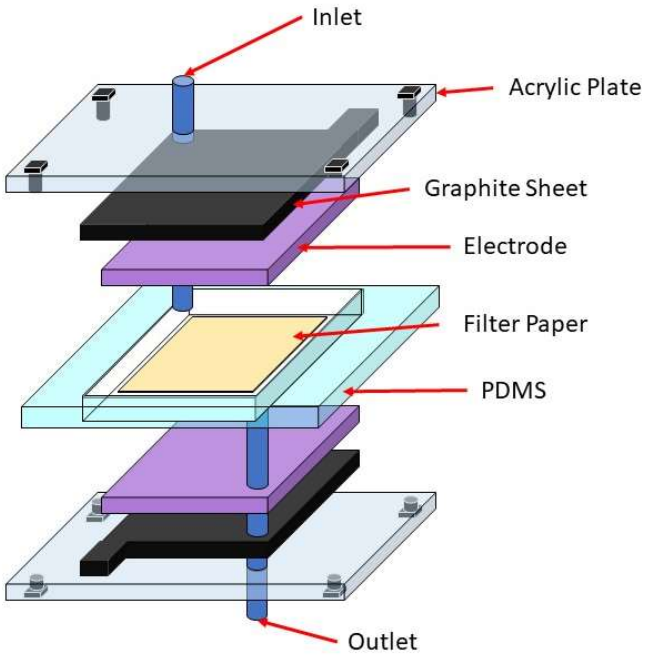

3.7 CDI System Setup

The CDI system was set up to simulate a flow operation of the CDI. During operation, liquid from the solution tank was pumped into the CDI, flowed out into the reservoir, and returned to the solution tank. During the adsorption phase, voltage difference would be applied across the CDI cell, supplied by the power supply. In the desorption phase, the power supply was disconnected to remove any applied voltage and induce desorption by the CDI cell. A data logger (Picolog®) and a resistance circuit (figure 3.4) were used to record voltage differences across the CDI cell and convert them into current profiles; they are represented as symbol M in figure 3.3. A conductivity meter was used to measure the conductivity of the effluent in the reservoir to observe the concentration changes of the solutions. The operating conditions (flow rate and applied voltage) will be varied to observe their effect on the metal removal performance and will be mentioned explicitly in each of the heavy metal removal sections.

Figure 3.3
CDI System Setup

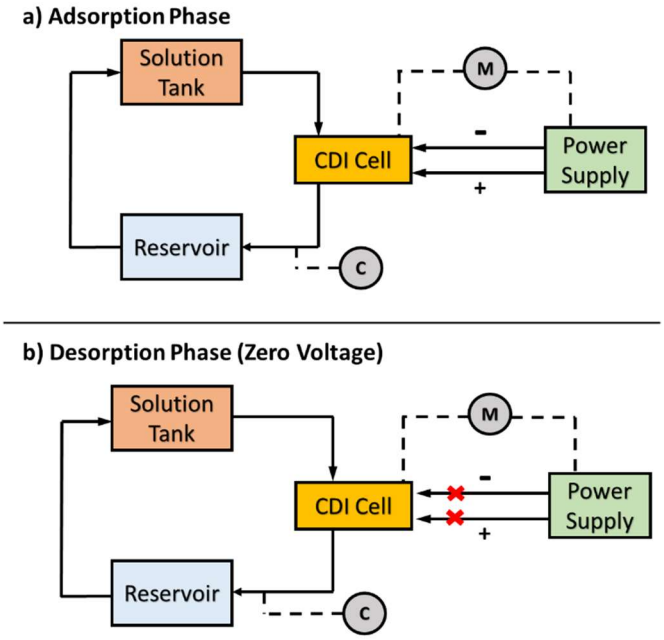

The resistance circuit, consisting of a 200 Ω resistor, was connected to the CDI cell and the datalogger as shown in figure 3.4. Because the datalogger available could only record voltage differences, the resistance circuit was implemented to ultimately obtain a current profile. The data logger would record the voltage difference at channel A and channel B where the difference between the two points would be the voltage difference across the resistor. The current could then be calculated using the resistance value of 200 Ω, compiled into current profiles which will be used to analyze the operating characteristic of the CDI.

Figure 3.4

Resistive Circuit Used During CDI Performance Tests

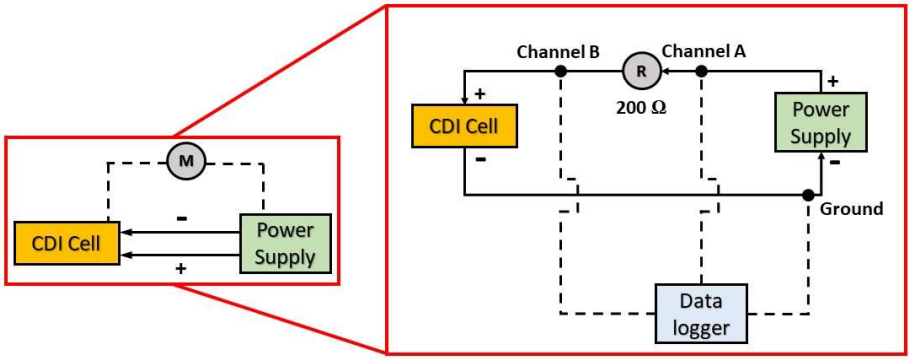

3.8 MnO_2/ACC Electrodes NaCl Adsorption in CDI Operation

The NaCl adsorption was performed to observe whether the electrodeposited MnO2/ACC electrodes achieve the objective of ion adsorption in CDI operation. Table salt was used to prepare 1000 ppm NaCl solution. The electrodeposited MnO_2/ACC electrodes were used in CDI operation with 0.8 V applied voltage and 10 ml/min flow rate. The calibration curve for the conductivity of the NaCl solution was prepared to obtain the concentration and adsorption profile for the CDI operation. The current profile of CDI operation was also recorded. The performance was evaluated using the ion adsorption capacity, ion adsorption rate, and charge efficiency.

Ion adsorption capacity and ion adsorption rate were used to describe the adsorption capability of the electrode material. Ion adsorption capacity is defined as the mass of adsorbed ion per mass of electrode while Ion adsorption rate is the rate at which ions are adsorbed per mass of electrode. Charge efficiency is defined as the ratio of adsorbed ions over charges density during adsorption cycles which allows the identification of the ratio between actual charges used for ion adsorption to charges transferred through the CDI system.

Ion Adsorption Capacity; $$q = \frac{(C_o - C_f)M}{m} V \qquad \ldots(3.2)$$

Where q = Ion adsorption capacity (mg/g)

C_0, C_f = Initial and final concentration of the ions (mM)

M = Molar mass of the metal salt (g/mol)

m = Mass of the electrode (g)

V = Volume of the solution (L)

Ion Adsorption Rate; $\dot{q} = \frac{q}{t_a}$ …(3.3)

Where $\dot{q}$ = Ion adsorption rate (mg/g·min)

t_a = Duration of adsorption phase of CDI (min)

Charge Efficiency; $\Lambda = \frac{q \cdot z \cdot F}{M \int_0^{t_a} I dt} \times 100$ …(3.4)

Where Λ = Charge efficiency

z = Number of charges on the ion

F = Faraday's constant (96485 C/mol)

I = Current during CDI adsorption (A)

3.9 Heavy Metal Removal Test – Individual Metal Species Removal

Metal ion solutions were used for the metal removal tests to observe the capability of the MnO_2/activated carbon cloth to adsorb each species from the solution under 1 hour of flow operation. As such, 4 batches of 1.5 mM metal solutions of copper, lead, cadmium, and chromium were prepared using $Cu(NO_3)_2$ (99%, Univar™), $Pb(NO_3)_2$ (99%, Univar™), $Cd(NO_3)_2 \cdot 4H_2O$ (99%, Loba Chemie™), and $Cr(NO_3)_3 \cdot 9H_2O$ (98%, Himedia™), respectively. During the operation, the applied voltage was varied between 0.8-1 V and the liquid flow rate was varied between 5-10 ml/min to observe the effects on the metal removal performance. Before the adsorption test of each species, the metal ion solution was pumped through the CDI cell for 30 minutes to ensure a steady-state of the CDI cell. This was done to ensure that the adsorption observed was due to the application of voltage difference. Raw activated carbon cloth which underwent only the cleaning process mentioned in section 3.2 was also used in the metal removal tests to compare its performance to the performance of MnO_2/ACC.

The calibration curves for each metal species' conductivity were prepared to obtain concentration profiles. The heavy removal performance of the electrode was evaluated using the ion adsorption capacity, ion adsorption rate, charge efficiency, and molar ion adsorption capacity. Molar ion adsorption capacity was used to allow for easier evaluation of ion adsorption capability between different metal species based on mole adsorbed than on mass adsorbed. The metric is calculated with the following equation.

Molar Ion Adsorption Capacity; $q_n = \frac{q}{M}$ …(3.5)

Where q_n = Molar ion adsorption capacity (mole/g)

3.10 Heavy Metal Removal Test – Multiple Metal Species Removal

The MnO_2/ACC electrodes in CDI were tested for heavy metal removal from the mixtures of multiple metal species at equal concentrations. The mixture was prepared from $Cu(NO_3)_2$ (99%, Univar™), $Pb(NO_3)_2$ (99%, Univar™), $Cd(NO_3)_2 \cdot 4H_2O$ (99%, Loba Chemie™), and $Cr(NO_3)_3 \cdot 9H_2O$ (98%, Himedia™) to achieve the concentration of 1.5 mM of copper, lead, cadmium, and chromium. The same adsorption condition in section 3.8 was used with operating conditions of 1.0 V applied voltage and 5 mL/min flow rate. In addition to the recording of conductivity over time, the final solution was analyzed for its compositions using Inductively coupled plasma atomic emission spectroscopy (ICP-AES, Shimadzu, ICPE-9820). The heavy removal performance of the electrode was evaluated using the ion adsorption capacity, ion adsorption rate, charge efficiency, and molar ion adsorption capacity.

3.11 Heavy Metal Removal under Multiple Cycle Operation

In this section, the heavy metal removal of MnO_2/ACC electrodes using CDI over multiple operating cycles was investigated. The CDI operation was performed on 4 batches of metal solution: copper, lead, cadmium, and chromium. The CDI system was operated with a flow rate of 10 ml/min, 1 V applied voltage during the adsorption phase, and 0 V during the desorption phase. Each phase was run for 10 minutes, added up to 20 minutes per cycle, and each test was run for a total of 16 cycles. The current profile and the charge ratio of each cycle were recorded to study its behavior during the operation and the changes after

each cycle. The charge ratio is a ratio of specific total passed charges of each cycle to that of the first cycle, where it can help identify the changes in behavior and performance of the CDI over multiple cycles. The total passed charges and the charge ratio of each cycle was calculated using the following equation:

$$Q = \frac{\int_{t_i}^{t_f} I dt}{m} \quad \ldots(3.6)$$

Where Q = Specific total passed charges (C/g)

t_f, t_i = Ending and Starting point of the adsorption phase

m = Mass of the electrode.

$$Charge\ ratio = \frac{Q_n}{Q_1} \quad \ldots(3.7)$$

Where Q_n = the specific total passed charge of the n^{th} cycle (C/g)

3.12 Chapter Summary

In this thesis, MnO_2 was deposited onto the activated carbon cloth via the cyclic voltammetry method. SEM, XRD, and cyclic voltammetry were used to identify the deposited MnO_2 and the effect of different depositing conditions on the properties of the electrodes. The CDI cell was then assembled using a 3 cm x 3 cm MnO_2/activated carbon cloth electrode for a CDI system with flow operation. The heavy metal removal capability on different metal species of the synthesized electrode was studied with metal solutions of copper, lead, chromium, and cadmium. The applied voltage and flow rate were varied between 0.8-1V and 5-10 ml/min during the operation to observe the effect on the metal removal. The metal removal capability was also tested on the mixture of multiple metal species. Lastly, the metal removal was performed on various metal solutions for 16 cycles each to observe the robustness of the electrode by observing the operation's current profiles.

CHAPTER 4
RESULT AND DISCUSSION

The MnO_2 deposited activated carbon cloth electrodes, referred to as MnO_2/ACC electrodes were fabricated under multiple conditions. The effects of the varying conditions were investigated using SEM, XRD, and cyclic voltammetry (CV) to identify the ideal properties for operation in capacitive deionization (CDI). And finally, the MnO_2/ACC CDI was operated with copper, cadmium, chromium, and lead metal solutions to investigate its heavy metal removal performance. The operating conditions of cell voltage, flow rate, and the multiple cycles operation were also investigated

4.1 Characterization of the Fabricated Electrodes

The fabricated MnO_2/ACC electrodes were characterized to investigate their properties and the effect of the deposition conditions: scanning electron microscope (SEM) for the surface morphology, x-ray powder diffraction (XRD) for the deposited MnO_2 structure, and cyclic voltammetry (CV) for capacitive behavior and areal capacitance. The MnO_2/ACC samples that were characterized are the samples from section 4.2.2.2 which were surface activated with 5% nitric acid aqueous solution, electrodeposited with cyclic voltammetry, and using Na_2SO_4 as a supporting electrolyte.

4.1.1 Surface Morphology of the MnO_2/ACC

Figure 4.1 shows the SEM images of the MnO_2/ACC samples under different deposition conditions, varying the deposition scan rate and the cycles. In all SEM results of the MnO_2/ACC sample, there are deposits of MnO_2 structure in different morphology. In figure 4.1 (a)-(b), the MnO_2/ACC sample deposited at 25 mV/s scan rate had small MnO_2 deposits distributed across the fiber of the activated carbon cloth, and uniform deposited structures formed between the fiber strands. While the MnO_2/ACC electrode deposited at 10 mV/s scan rate in figure 4.1 (c)-(d), had sporadically distributed larger deposited structure on the fiber and less deposition between the fiber strands. The results indicate that the higher scan rate, which has a shorter deposition period, favors nucleation over the crystal growth, leading to the spread of small MnO_2 deposits in comparison to the deposition at a lower scan rate which has a longer deposition period.

Figure 4.1

SEM Images of MnO_2/ACC Samples

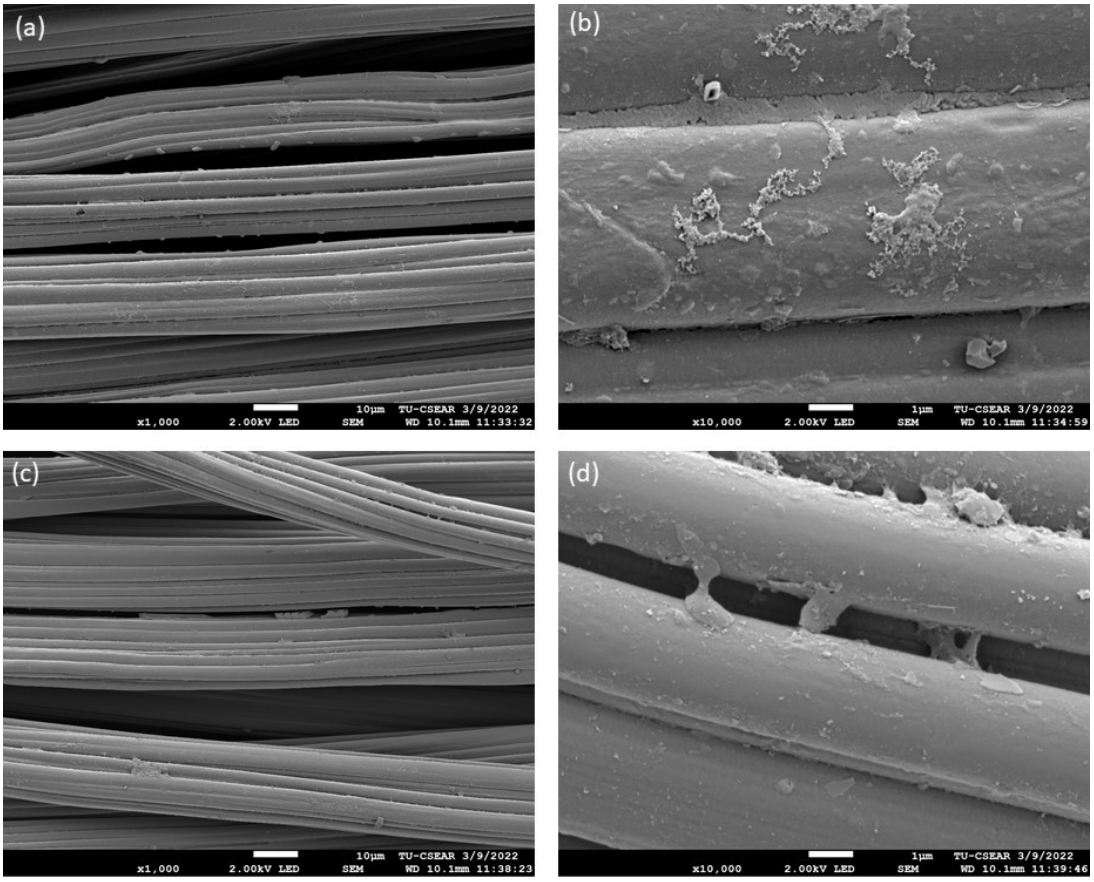

Note. SEM images of MnO_2/ACC samples deposited at 25 mV/s with (a)1,000x and (b)10,000x magnification, and deposited at 10 mV/s with (c)1,000x and (d)10,000x magnification.

In figure 4.2 (a)-(b), the MnO_2/ACC sample was prepared at 25 mV/s scan rate and 10 deposition cycles. The figures show fewer small deposits across the fibers but more uniform deposits between the fiber strands. The results indicate that, although the higher scan rate favors nucleation, the increased deposition cycles allow for the crystal growth to occur and develop uniformly across the fibers of the activated carbon cloth.

Figure 4.2

SEM Images of MnO_2/ACC and Raw ACC Samples

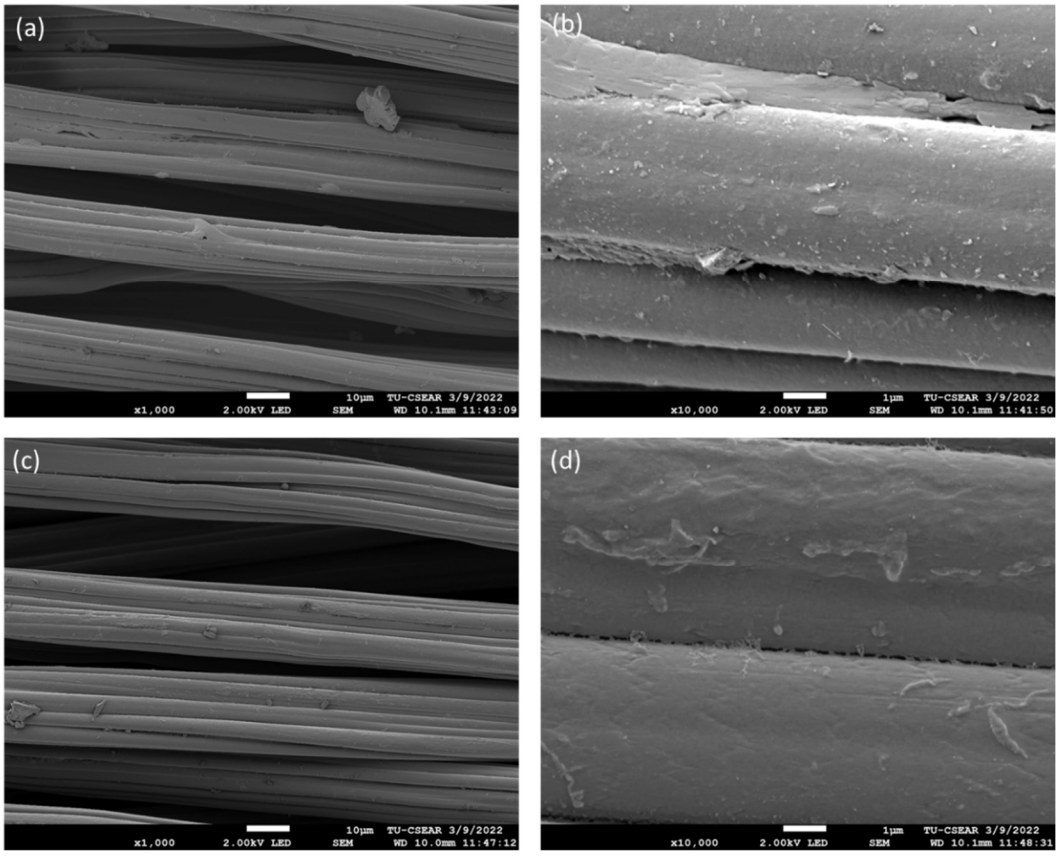

Note. SEM images of a MnO_2/ACC sample deposited at 25 mV/s and 10 cycles with (e)1,000x and (f)10,000 magnification, and a raw ACC sample with (g)1,000x and (h)10,000x magnification.

4.1.2 Crystal Structure of MnO_2/ACC

The XRD results in figure 4.3 show peaks at 24° and 44° found in both raw ACC and MnO_2/ACC which can be attributed to the crystal planes, (002) and (100), of the graphitic planes in the carbon cloth(Thamilselvan et al., 2015). The weak peaks at 32° and 34° can be attributed to the presence of the deposited Mn_2O_3 as well (Chang et al., 2004) which increases with longer deposition time as seen in the sample deposited at 10 mV/s. In agreement with past works on the electrodeposition of MnO_2, the depositing conditions show no significant effect on the samples' XRD pattern.

Figure 4.3

XRD Patterns of MnO_2/ACC Samples

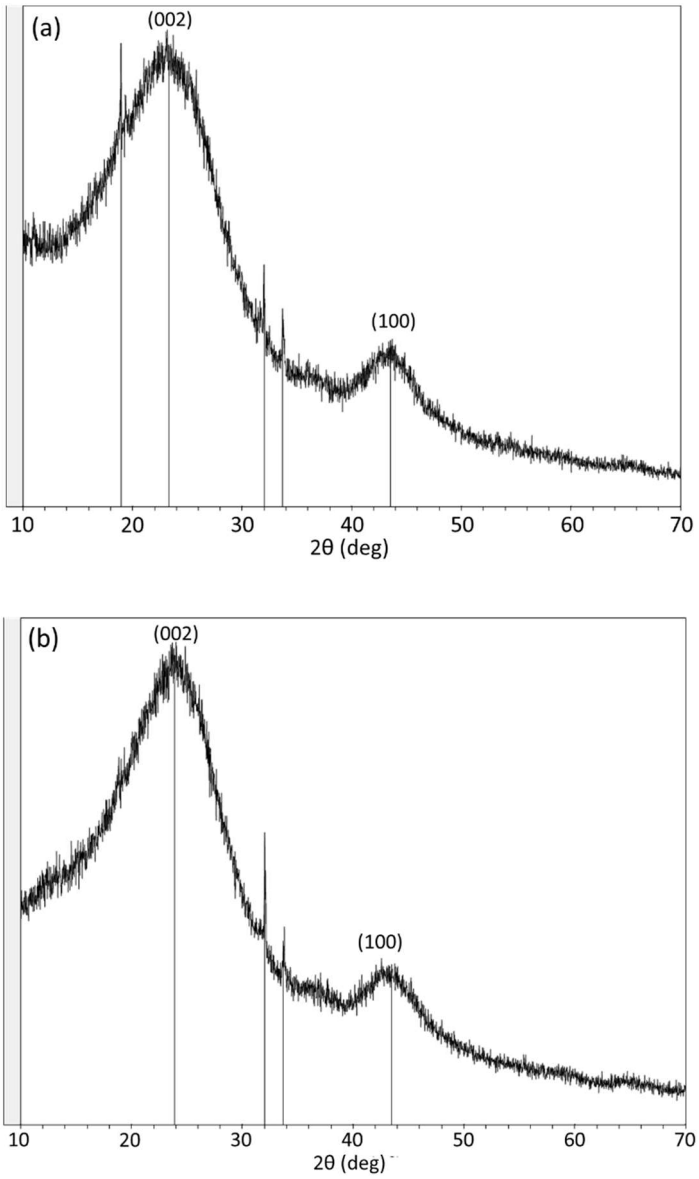

Note. XRD patterns of MnO_2/ACC samples deposited at 10 deposition cycles and (a) 25 mV/s and (b) 10 mV/s deposition scan rate.

4.2 Electrochemical Characterization of the Fabricated Electrodes

The fabricated MnO_2/ACC electrodes were characterized using cyclic voltammetry to investigate their electrochemical characteristics and the effect of the deposition conditions.

4.2.1 MnO_2/ACC Electrodes Electrodeposited Using Amperometry Method.

MnO_2/ACC samples were prepared using amperometry method, by varying the voltage between 0.8 – 1.0 V and electrodeposition duration between 5 – 10 minutes. Its cyclic voltammogram and the areal capacitance are shown in figure 4.4 and table 4.1. The voltammograms showed leaf-like shapes in all depositing conditions, indicating that the MnO_2 deposition at different conditions did not cause significant changes in the capacitive behavior from that of the raw ACC. The leaf-like shape voltammogram is a common behavior for a porous supercapacitor due to the slow movement of ions in and out of the porous structure, causing the voltammogram to deviate from a rectangular voltammogram of a capacitor. Thus, these voltammograms indicate a slow charge-discharge of the MnO_2/ACC electrodes which was not improved by the deposition of MnO_2 or the varied deposition conditions. The reduced deposition time from 10 to 5 minutes decreased the areal capacitance from 68.75 mF/cm^2 to 33.50 mF/cm^2. On the other hand, the areal capacitance was increased from 68.75 mF/cm^2 to 87.75 mF/cm^2 when the applied voltage was increased from 0.8 V to 1.0 V.

Figure 4.4

Voltammograms of MnO_2/ACC Electrodes Electrodeposited Using Amperometry Method

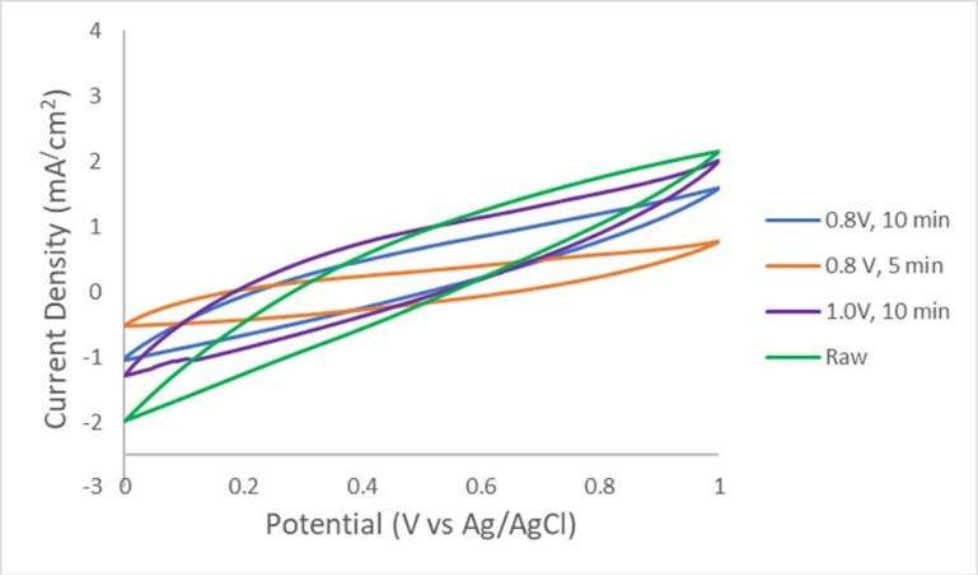

Note. Cyclic voltammogram of MnO_2/ACC electrodes scanned at 10 mV/s. The MnO_2/ACC electrodes were deposited using amperometry method.

Table 4.1

Areal Capacitance of MnO_2/ACC Electrodes Using Amperometry Method

Fixed Voltage (V)	Deposition Time (minutes)	Areal Capacitance (mF/cm^2)
Raw		107.25
0.8	5	33.50
	10	68.75
1.0	10	87.75

Note. The capacitances were obtained from voltammograms scanned at 10 mV/s

The effect of the depositing conditions on the areal capacitance can be attributed to the amount of total passed charges. The increased deposition time and applied voltage both contributed to the higher amount of total passed charges, leading to more deposition of

MnO_2, and higher areal capacitance. This is in accordance with many works on MnO_2 deposition using amperometry method. However, the areal capacitance achieved was still lower compared to raw ACC, which indicated that the deposition of MnO_2 was restricting the electrochemical property of the samples. After the electrodeposition, yellow contaminants (figure 4.5) were also observed on the surface of the samples as well. Both characteristics were similarly observed in the samples discussed in the next section, which were prepared in the same depositing solution but electrodeposited using cyclic voltammetry. And since both characteristics were similarly observed in both batches, they will be further discussed in the next section instead.

Figure 4.5

Formation of Yellow Contaminants on the MnO_2/ACC Samples Prepared Using $Na(CH_3COO)$ as a Supporting Electrolyte.

4.2.2 MnO_2/ACC Electrodes Electrodeposited Using Cyclic Voltammetry Method

***4.2.2.1* MnO_2/ACC Electrodes Electrodeposited with $Na(CH_3COO)$ as a Supporting Electrolyte.** Based on the work of (Prasad & Miura, 2004; Shinomiya et al., 2006), MnO_2 electrodes electrodeposited using cyclic voltammetry were able to achieve

higher specific capacitance compared to other electrodeposition methods. And a positive correlation between the specific capacitance of the electrode with its ion adsorption performance in CDI operation has been established in many works (C. Hu et al., 2015, C. Zhao et al., 2017). Therefore, MnO_2/ACC's electrodeposition method was changed to cyclic voltammetry in favor for a higher specific capacitance. As mentioned before, this batch of samples also showed formations of yellow contaminants on the surface after the electrodeposition as shown in figure 4.5. The yellow contaminants would also diffuse into the solution when performing cyclic voltammetry characterization, causing the voltammogram to translate vertically as shown in figure 4.6. The formation of the yellow contaminants was attributed to the use of $Na(CH_3COO)$ as a supporting electrolyte. This was found when any samples electrodeposited with Na_2SO_4 did not form yellow contaminants on their surface as shown in figure 4.6.

Figure 4.6

Electrodeposited Samples Using Na_2SO_4 as a Supporting Electrolyte

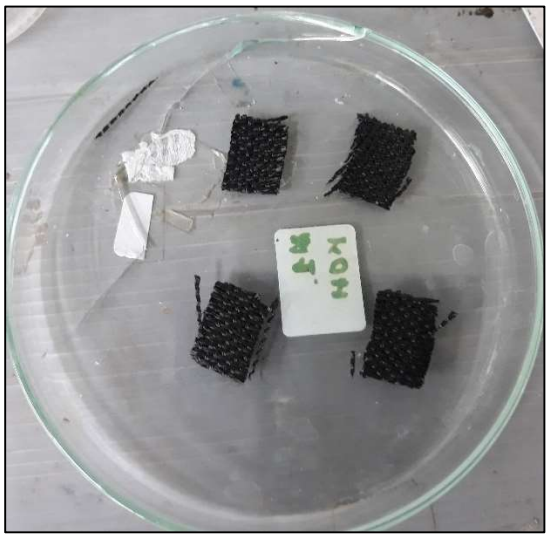

The cyclic voltammogram and the areal capacitance of the electrodeposited samples are shown in figure 4.7 and table 4.2. Despite the changes in the electrodeposition method, the voltammograms of the samples still did not show significant changes from that of the raw ACC. Thus, it indicates that the different electrodeposition method does not impose

significant change on the voltammogram of the samples. In terms of areal capacitance, the highest areal capacitance of 49.50 mF/cm^2 was observed in a batch prepared at the depositing scan rate of 25 mV/s, while the batch prepared at 50 and 10 mV/s depositing scan rate achieved areal capacitance of 42.31 mF/cm^2 and 12.98 mF/cm^2, respectively.

When the deposition cycle was increased from 5 cycles to 10 cycles, varying results were observed based on the depositing scan rate. For the batch with a depositing scan rate of 25 mV/s and 10 deposition cycles, the areal capacitance decreased to 44.25 mF/cm^2. This indicated a negative correlation between the areal capacitance and the deposition cycle. However, for the batch with a depositing scan rate of 10 mV/s and 10 deposition cycles, the areal capacitance increased to 26.50 mF/cm^2. This indicated a positive correlation between the areal capacitance and the deposition cycle. Thus, it can be concluded that the effect of the deposition cycles on the areal capacitance also depended on the depositing scan rate as well.

Figure 4.7

Voltammograms of MnO_2/ACC Electrodes Electrodeposited with $Na(CH_3COO)$ as a Supporting Electrolyte

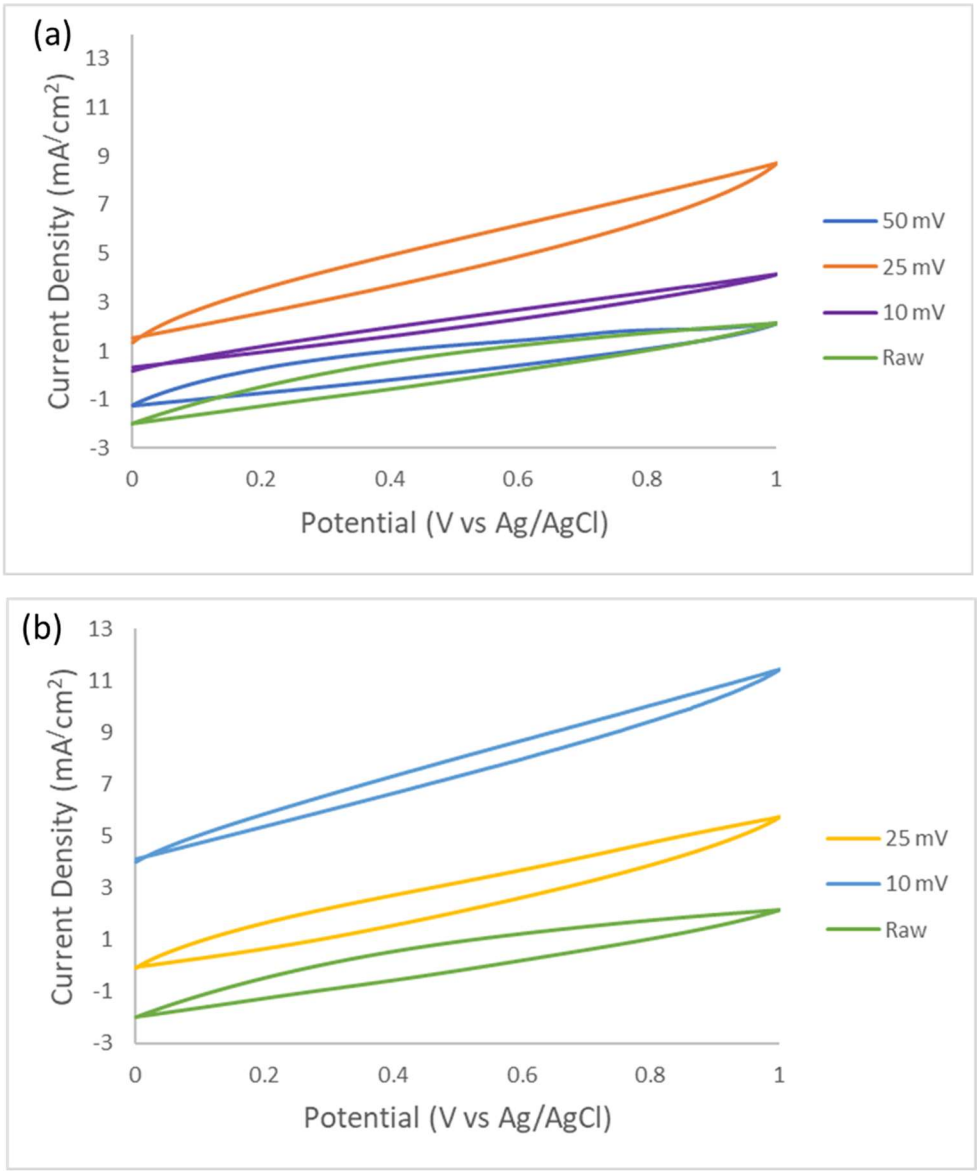

Note. Cyclic voltammogram of MnO_2/ACC electrodes scanned at 10 mV/s. The MnO_2/ACC electrodes were deposited at (a) 5 deposition cycles and (b) 10 deposition cycles.

Table 4.2

Areal Capacitance of MnO_2/ACC Electrodes with $Na(CH_3COO)$ as a Supporting Electrolyte

Deposition Cycle	Deposition Scan Rate (mV/s)	Areal Capacitance (mF/cm^2)
Raw		107.25
5 cycles	50 mV/s	42.31
	25 mV/s	49.50
	10 mV/s	12.98
10 cycles	25 mV/s	44.25
	10 mV/s	26.50

Note. The capacitances were obtained from voltammograms scanned at 10 mV/s

The MnO_2/ACC samples prepared using $Na(CH_3COO)$ as a supporting electrolyte exhibited a drastic decrease in areal capacitance compared to the raw ACC. This is a similar restricting effect of the electrodeposited MnO_2 on the areal capacitance observed in the last section. The restricting effect is due to the excessive formation of yellow contaminants, which plugged up the pore structure and interfered with the electrochemical property of the samples. The work of (Broughton & Brett, 2005) showed that the use of $Na(CH_3COO)$ as a supporting electrolyte caused the spontaneous formation of manganese oxide in the depositing solution.

This characteristic was also observed during the preparation of the depositing solutions in our work where the yellow contaminants, now identified as oxides of manganese, spontaneously formed. The work of (Broughton & Brett, 2005) also mentioned the reduced depositing voltage of MnO_2 when $Na(CH_3COO)$ was used, leading to a longer period of deposition for cyclic voltammetry electrodeposition. Thus, these reasons can be used to explain the excessive formations of oxides of manganese observed only in samples prepared using $Na(CH_3COO)$ as a supporting electrolyte.

The effect of the different depositing conditions on the areal capacitance can also be explained by the formation of the oxides of manganese. Samples deposited at 10 mV/s depositing scan rate exhibited much lower areal capacitance compared to other scan rates can be attributed to the longer deposition time allowing for larger formations of oxides which hampered its electrochemical characteristics. When the deposition cycles were increased to 10 cycles, samples deposited at 25 mV/s scan rate also shown dropped in areal capacitance due to the longer deposition time. However, for samples deposited at 10 deposition cycles and 10 mV/s scan rate, the increase in areal capacitance was largely contributed by the layer of excessive oxide formed and not by the porous structure of the ACC. The results show that the use of $Na(CH_3COO)$ as a supporting electrolyte greatly hampers the electrochemical property of the MnO_2/ACC despite the varying depositing conditions. As such, the supporting electrolyte was then changed to Na_2SO_4 from that point on.

4.2.3 MnO_2/ACC Electrodes Electrodeposited with Na_2SO_4 as a Supporting Electrolyte

4.2.3.1 **MnO_2/ACC Electrodes Surface Activated with KOH.** For the samples prepared using Na_2SO_4 as a supporting electrolyte and surface activated with KOH, their cyclic voltammogram and areal capacitance are shown in figure 4.8 and table 4.3. In comparison to the capacitive behavior of the raw ACC, the MnO_2/ACC samples deposited under this condition showed no significant change in their capacitive behavior as well. Thus, the change of supporting electrolyte from $Na(CH_3COO)$ to Na_2SO_4 did not cause significant changes to the samples' voltammogram and capacitive behavior. As for the effect of depositing conditions on the areal capacitance, 25 mV/s depositing scan rate batches showed a similar level of areal capacitance to the raw ACC electrode at 97.25 mF/cm^2 and 83.25 mF/cm^2 for batches with 5 and 10 depositing cycles, respectively. While for 10 mV/s depositing scan rate samples, the samples showed lower areal capacitance of 60.50 mF/cm^2, with further reduction in batches with increased depositing cycle down to 45.75 mF/cm^2.

Figure 4.8

Voltammograms of MnO_2/ACC Electrodes Surface Activated with KOH

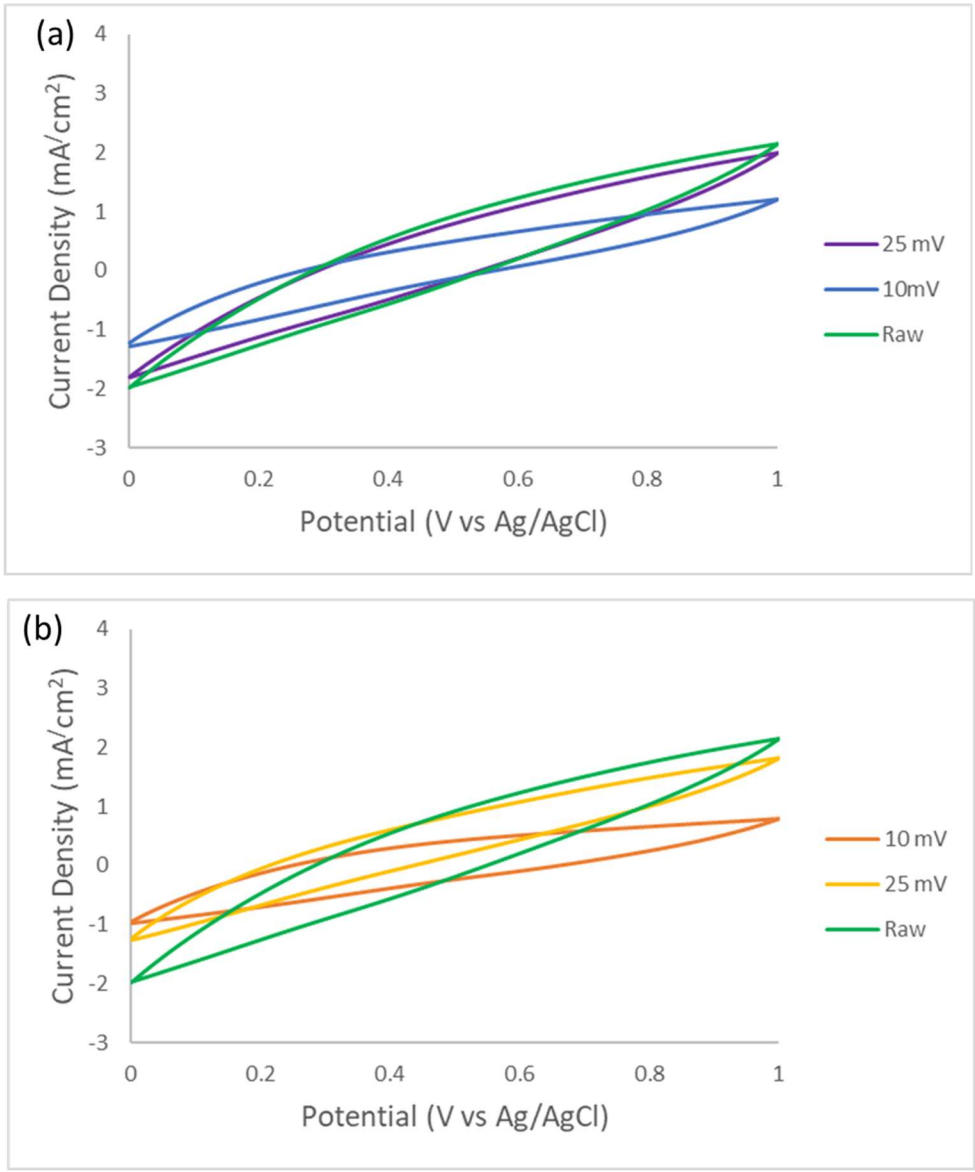

Note. Cyclic voltammogram of MnO_2/ACC electrodes scanned at 10 mV/s. The MnO_2/ACC electrodes were deposited at (a) 5 deposition cycles and (b) 10 deposition cycles.

Table 4.3

Areal Capacitance of MnO_2/ACC Electrodes Surface Activated with KOH

Deposition Cycle	Deposition Scan Rate (mV/s)	Areal Capacitance (mF/cm^2)
Raw		107.25
5 cycles	25 mV/s	97.25
	10 mV/s	60.50
10 cycles	25 mV/s	83.25
	10 mV/s	45.75

Note. The capacitances were obtained from voltammograms scanned at 10 mV/s

The areal capacitances of the MnO_2/ACC samples were positively correlated to the depositing scan rate. This can be explained by the reasonings provided in the work of (Prasad & Miura, 2004; Shinomiya et al., 2006) that higher depositing scan rates allow for a MnO_2 deposition of less density and higher porosity, which ultimately increased the capacitance. However, increasing deposition cycles would reduce the areal capacitance of the samples instead. Their relationship can be attributed to the lower amount of oxygen-containing functional groups modified on the surface due to using KOH for activation (Lee, 2015). With fewer sites of these functional groups, MnO_2 would deposit close together instead of spreading out, forming densely packed lattice structures that reduce the capacitance instead. Despite switching the supporting electrolyte to Na_2SO_4, the electrodeposited MnO_2/ACC samples still did not achieve higher areal capacitance than a raw ACC nor have consistently repeatable characteristics. It was only after changing to surface activating the samples with 5% nitric acid solution that samples with areal capacitance higher than a raw ACC can be consistently reproduced and higher capacitance could be achieved when the deposition cycles were increased.

MnO_2/ACC electrodes activated with 5% HNO_3. The capacitive behavior of the MnO_2/ACC electrode can be observed from the cyclic voltammogram of the electrode fabricated at various synthesis conditions. In figure 4.9, the electrodes exhibited leaf-like voltammograms similarly in all samples, indicating that the deposition conditions did not cause significant changes in the capacitive behavior. A conclusion can be made that the electrodeposition methods, the types of supporting electrolytes, and the surface activation methods used in this work do not provide significant effects in changing the voltammogram and capacitive behavior of the MnO_2/ACC samples.

Considering the areal capacitances shown in table 4.4, the areal capacitance was higher in samples with higher depositing scan rates, achieving the highest value of 139.55 mF/cm^2 for a depositing scan rate of 50 mV/s, and 128.54 mF/cm^2 and 121.81 mF/cm^2 for a depositing scan rate of 25 and 10 mV/s, respectively. In terms of the deposition cycle, the effects varied based on the deposition scan rate. When the deposition cycle was increased, the electrode's areal capacitance increased from 128.54 mF/cm^2 (5 cycles) to 134.51 mF/cm^2 (10 cycles) at a 25 mV/s deposition scan rate. While for the electrode deposited at a 10 mV/s scan rate, the areal capacitance decreased from 121.81 mF/cm^2 (5 cycles) to 96.38 mF/cm^2 (10 cycles).

Comparing the areal capacitance of the MnO_2/ACC deposited with amperometry method in section 4.2.1, It can be seen that electrodeposition using cyclic voltammetry can produce samples with higher areal capacitance than using amperometry. Between all of the studied depositing conditions, the highest areal capacitance of 134.51 mF/cm^2 was achieved with the synthesis conditions of 25 mV/s scan rate and 10 cycle deposition. Thus, the MnO_2/ACC electrodes used for the CDI operation experiment were prepared with these specific depositing conditions.

Figure 4.9

Voltammograms of MnO_2/ACC Electrodes Activated with 5% HNO3 and Na2SO4 as Supporting Electrolyte

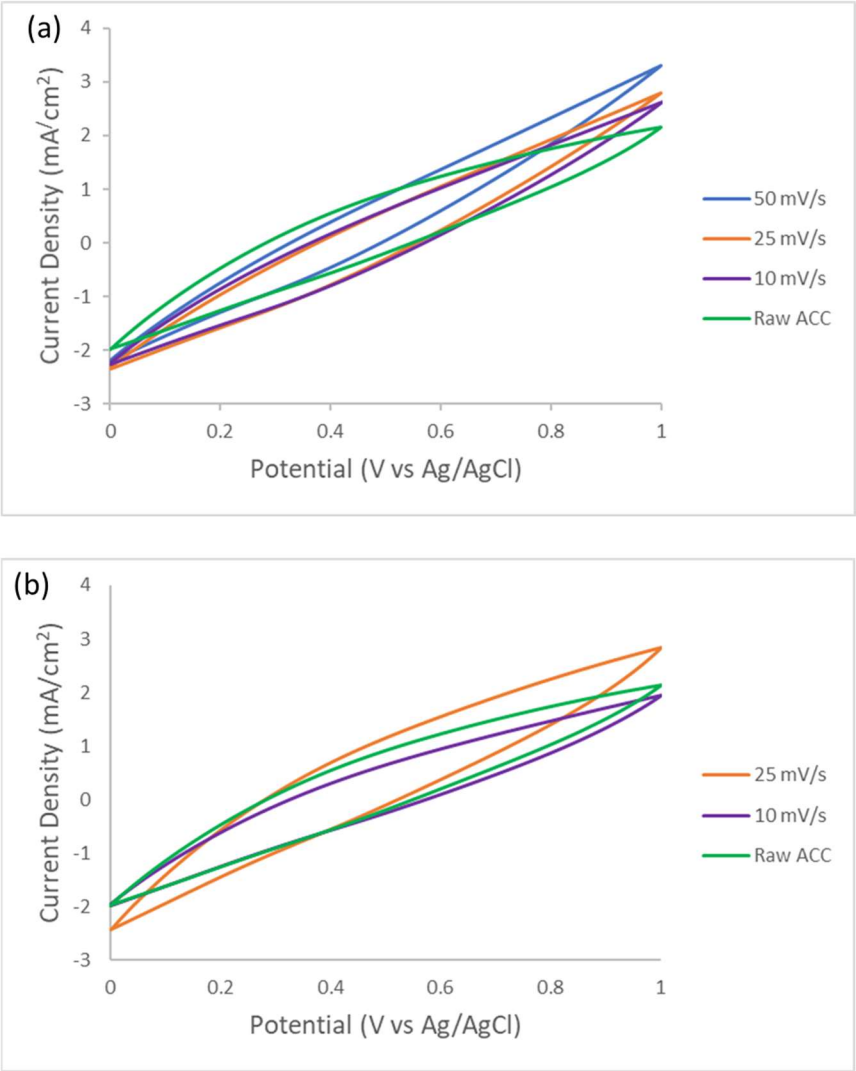

Note. Cyclic voltammogram of MnO_2/ACC electrodes scanned at 10 mV/s. The MnO_2/ACC electrodes were deposited at (a) 5 deposition cycles and (b) 10 deposition cycles.

Table 4.4

Areal Capacitance of MnO_2/ACC Electrodes Activated with 5% HNO3 and Na2SO4 as Supporting Electrolyte

Deposition Cycle	Deposition Scan Rate (mV/s)	Areal Capacitance (mF/cm^2)
Raw		107.25
5 cycles	50 mV/s	139.55
	25 mV/s	128.54
	10 mV/s	121.81
10 cycles	25 mV/s	134.51
	10 mV/s	96.38

Note. The capacitances were obtained from voltammograms scanned at 10 mV/s

The increased capacitance with the scan rate is in agreement with the work of (Prasad & Miura, 2004; Shinomiya et al., 2006) who related the higher scan rate with lower deposition density and higher porosity, leading to improved capacitance. However, due to the porous nature of the carbon substrate, very high scan rate can lessen the travel time of the precursors into the porous structure, depositing near the entrance, and plugging the pore instead. The plugging of the hole by MnO_2 deposits would inadvertently reduce the effective surface area and the adsorption capacity of the electrodes. Thus, an ideal level of depositing scan rate should be identified to achieve the highest areal capacitance. As for the effect of the deposition cycle, the increased cycles can be tied to increased deposition and formation of MnO_2 structure which can improve the capacitance. However, with the previous explanation, longer deposition at lower scan rate leads to longer deposition time, which produces MnO_2 crystal structures of lower porosity and denser packing. MnO_2 deposited in this manner would have lower areal capacitance. Therefore, further studies should be made to identify the ideal deposition scan rate and cycles in which the capacitive properties can still be improved without impeding its adsorption performance in CDI.

4.3 MnO_2/ACC Electrodes NaCl Adsorption in CDI Operation

The NaCl adsorption was performed to observe whether the electrodeposited MnO_2/ACC electrodes, the fabricated CDI cell, the CDI system, and the designed CDI operation can together achieve ion adsorption. The CDI cell was assembled with the MnO_2/ACC electrode as one of the electrodes and the CDI system was set up and operated according to sections 3.7 and 3.8 in chapter 3. The fabricated CDI cell and system were set up as shown in appendix A. The concentration profile, the adsorption profile, and the current profile of the NaCl adsorption are shown in figure 4.10.

The NaCl solution was initially prepared at 1000 ppm or 17.11 mM. After 1 hour of adsorption at 0.8 V and 10 ml/min flow rate, the concentration was reduced to 15.76 mM and the adsorption capacity reached 14.25 mg/g. The CDI operation also achieved a charge efficiency of 50.79%. Although the current profile of the adsorption phase exhibit common behavior for CDI operation, the current profile of the desorption phase exhibits a much smaller profile and lower specific total passed charges of only 0.75 mC/g compared to the adsorption phase of 20.52 mC/g.

This is attributed to a much slower desorption mechanism due to the adsorption of ions by the MnO_2/ACC. A process composed of a faster electrical double layer and a slower pseudocapacitive intercalation. But since most of the passed charges recorded should be attributed to the movement of the desorbed ions, the desorption phase should also achieve much higher charge efficiency as well. Still, these results showed that the electrodeposited MnO_2/ACC electrodes, the fabricated CDI cell, the CDI system, and the designed CDI operation can successfully achieve ion adsorption from NaCl solution.

Figure 4.10

Concentration, Adsorption, and Current Profile of NaCl

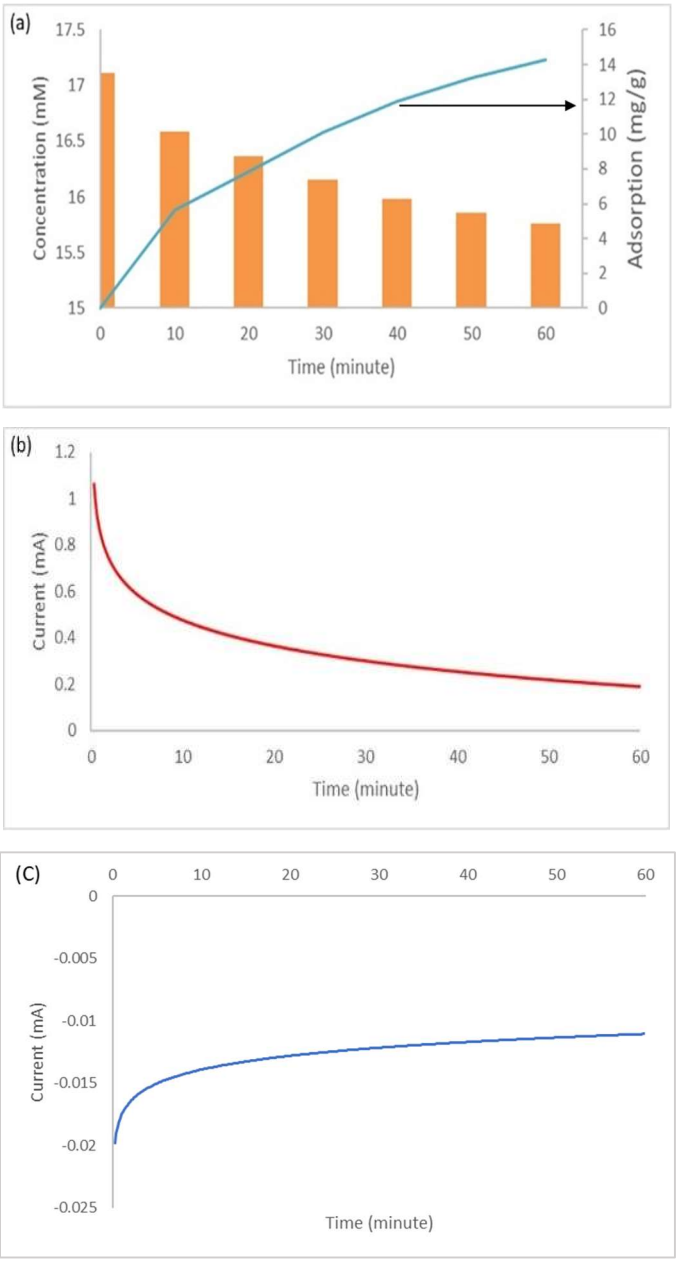

Note. (a) concentration and adsorption profile, and the current profiles of (b) the adsorption phase and (c) the desorption phase

Table 4.5
Performance Metrics for NaCl Adsorption

Ion Species	Operating Conditions: AV (V), FR (mL/min)*	Ion Adsorption Capacity (mg/g)	Ion Adsorption Rate (mg/g·min)	Charge Efficiency
NaCl	0.8 V, 10 ml/min	14.25	0.24	50.79

4.4 Heavy Metal Removal Test – Individual Removal

In table 4.6, MnO_2/ACC electrode showed its adsorption selectivity for each metal species in descending order of Cr^{3+}, Pb^{2+}, Cu^{2+}, and Cd^{2+}, achieving their highest adsorption capacity of 8.76, 6.48, 3.64, and 3.41 mg/g. And when the CDI operating conditions of cell voltage and flow rate were changed, the effects on the adsorption can be observed based on the adsorption capacity. When the flow rate was increased from 5 ml/min to 10 ml/min, the adsorption capacity of Cr^{3+}, Pb^{2+}, Cu^{2+}, and Cd^{2+} became 6.33, 4.36, 2.42, and 2.43 mg/g, reduced by 28%, 33%,33%, and 29%, respectively. When the cell voltage was reduced from 1 V to 0.8 V, the adsorption capacity of Cr^{3+}, Pb^{2+}, Cu^{2+}, and Cd^{2+} became 7.14, 5.29, 2.97, and 2.43 mg/g, reduced by 18%, 18%, 18%, and 29%, respectively. The concentration, adsorption capacity, and current profiles are shown in figures 4.11, 4.12, and 4.13. In agreement with the works of (Huang et al., 2016), the reason for the difference in adsorption of each species is a combination of multiple factors: the hydrated radius, the charge size, and the favorable adsorption mechanism. In this case, Cr^{3+} holds the largest charge and favors faster physical adsorption, resulting in the highest adsorption capacity. And between metal ions of equal charge size (Pb^{2+}, Cd^{2+}, Cu^{2+}), the hydrated radius would have a larger contribution in dictating their adsorptions, with species with larger hydrated radius would have slower ion movement and less adsorption by the CDI. Since the hydrated radii of these metal ions are in the ascending order of Pb^{2+}, Cu^{2+}, and Cd^{2+}, the ion adsorption capacities of these metal species shown in table 4.6 agree with this reasoning.

Table 4.6

Performance Metrics of Individual Metal Removal under Varying Operating Conditions

Metal Species	Operating Conditions: AV (V), FR (mL/min)*	Ion Adsorption Capacity (mg/g)	Molar Ion Adsorption Capacity (µmole/g)	Ion Adsorption Rate (mg/g·min)	Charge Efficiency
Chromium	1.0 , 5	8.76	36.80	0.15	2.57%
	1.0 , 10	6.33	26.61	0.11	1.86%
	0.8 V, 5	7.14	30.01	0.12	2.89%
	1.0 V, 5, Raw**	6.87	28.88	0.11	3.69%
Lead	1.0 V, 5	6.48	19.55	0.11	1.89%
	1.0 V, 10	4.36	13.17	0.07	1.27%
	0.8 V, 5	5.29	15.96	0.09	2.52%
	1.0 V, 5, Raw**	4.63	13.97	0.08	2.24%
Copper	1.0 V, 5	3.64	19.41	0.06	1.01%
	1.0 V, 10	2.42	12.92	0.04	0.67%
	0.8 V, 5	2.97	15.85	0.05	1.15%
	1.0 V, 5, Raw**	1.76	9.39	0.03	0.75%
Cadmium	1.0 V, 5	3.41	14.42	0.06	1.13%
	1.0 V, 10	2.43	10.22	0.04	1.06%
	0.8 V, 5	2.43	10.21	0.04	1.59%
	1.0 V, 5, Raw**	1.14	4.81	0.02	0.59%

Note. * AV = Applied Voltage, FR = Flow Rate. ** "Raw" indicates the use of raw activated carbon as electrodes instead of MnO_2/ACC electrodes.

Figure 4.11

Concentration Profile of Individual Metal Removal

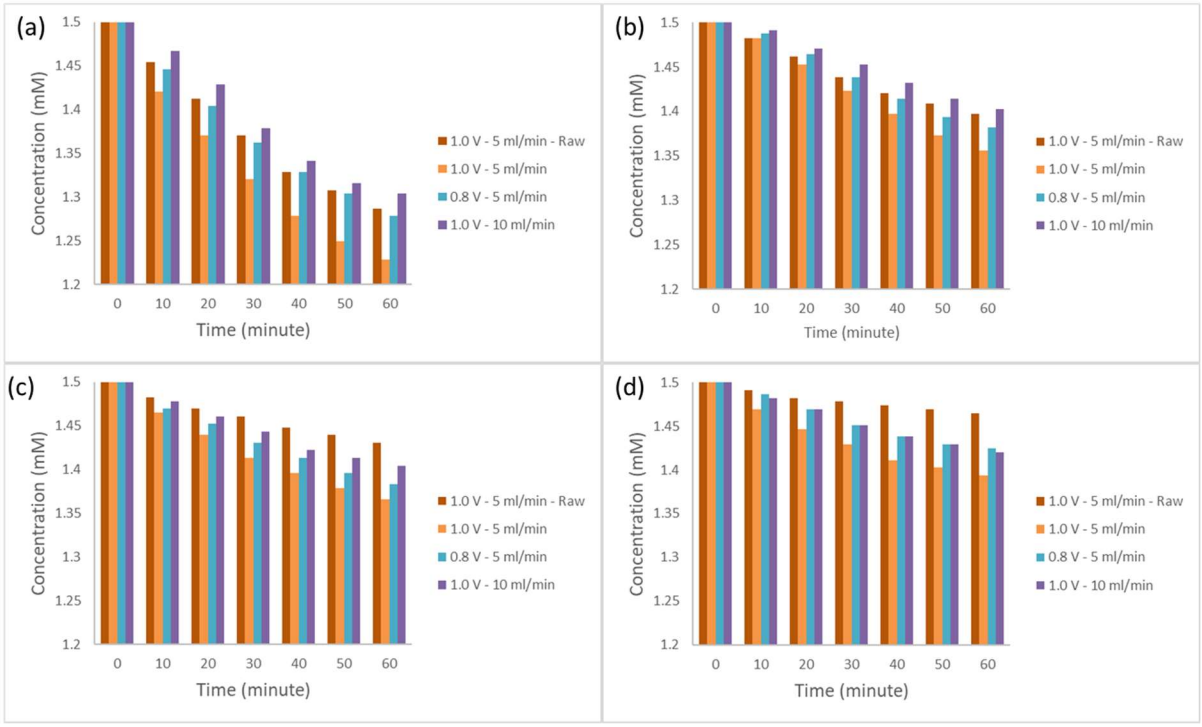

Note. concentration profiles of heavy metal removal of (a) Chromium, (b) Lead, (C) Copper, and (d) cadmium via CDI under varying operating conditions

.

Figure 4.12

Adsorption Profile of Individual Metal Removal

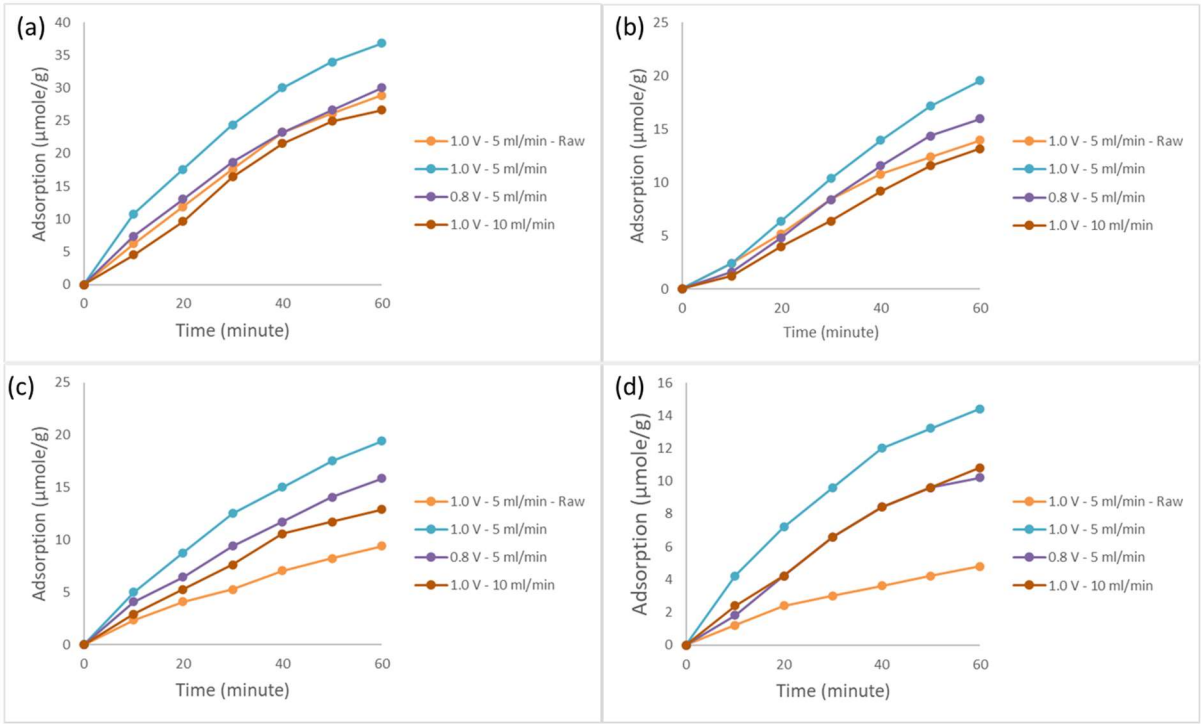

Note. adsorption profiles of heavy metal removal of (a) Chromium, (b) Lead, (C) Copper, and (d) cadmium via CDI under varying operating conditions.

Figure 4.13

Current Profile of Individual Metal Removal

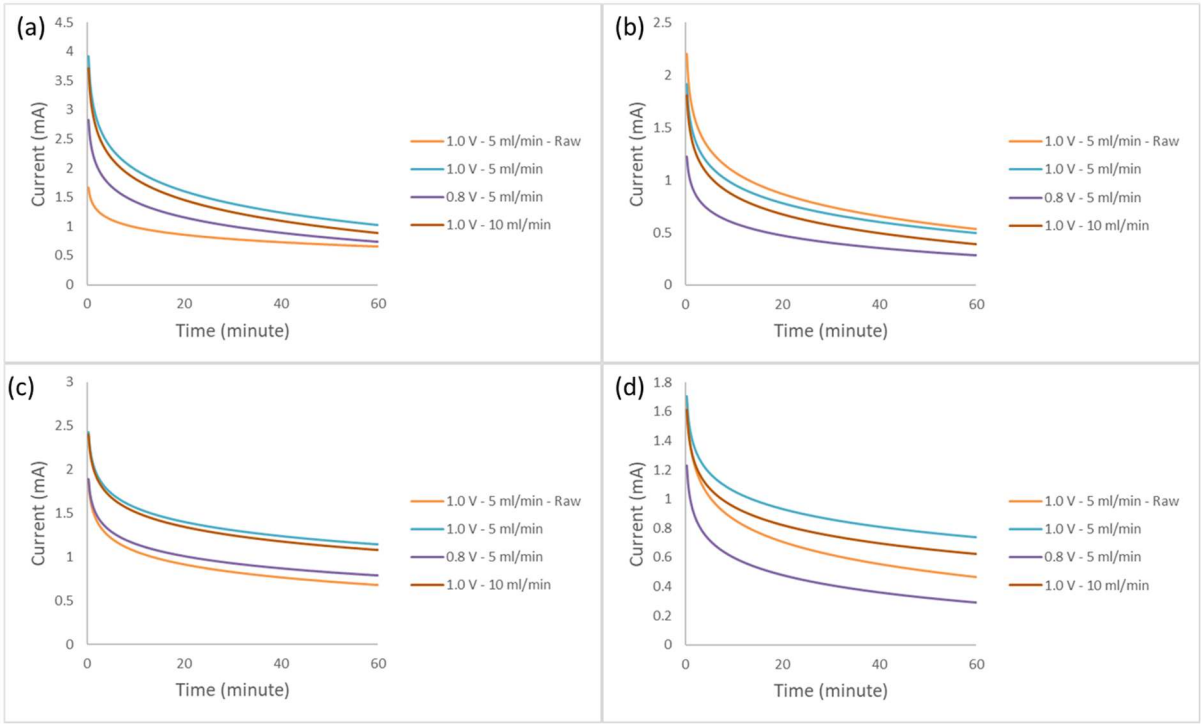

Note. Current profiles of heavy metal removal of (a) Chromium, (b) Lead, (C) Copper, and (d) cadmium via CDI under varying operating conditions.

Based on the effect of the operating conditions, the flow rate shows to negatively affect the heavy metal removal performance of the CDI. This can be explained as the higher flow rate reducing the traveling time of the ions from the bulk flow to the electrode. And the effect can be considered unrelated to the nature of the metal ions as there are no substantial differences when the metal specie was varied. As for the effect of the cell voltage, the adsorption of Cd^{2+} was the most affected. The results are in agreement with the work of (Huang et al., 2016) which showed that the adsorption of Cd^{2+} relies more on electrosorption compared to other metal species, and therefore would be the most affected by the changes in applied voltage. And thus, it also indicates that the other three species are less reliant on electrochemical adsorption due to a lower reduction in ion adsorption capacity when applied voltage was reduced.

In terms of charge efficiency, the efficiency was reduced when the flow rate was increased as observed in the adsorption of each metal species. As the ion adsorption decreases from the increased flow rate while the current profiles display no significant changes, the charge efficiency, therefore, becomes lower compared to operation at a lower flow rate. The charge efficiency also decreased when applied voltage was increased which contradicts the behavior normally observed in porous carbon electrodes (R. Zhao et al., 2010). This can be a characteristic of the MnO_2/ACC electrode as the raw ACC electrode was able to achieve higher energy efficiency at the same operating conditions for the adsorptions of chromium and lead. The adsorptions of cadmium and copper are exceptions due to poor adsorption by raw ACC.

4.5 Heavy Metal Removal Test – Competitive Metal Removal

In table 4.7, the adsorption capacities of each metal species by MnO_2/ACC electrode are shown. The conductivity and the differential conductivity were also shown in figure 4.14. The removal performance under competitive conditions for Cr^{3+}, Pb^{2+}, Cu^{2+}, and Cd^{2+} showed diminished adsorption capacities of 2.79, 5.26, 3.52, and 1.43 mg/g, respectively, which decreased by 68%, 19%, 3%, and 58%, respectively, in comparison to the adsorption of individual metal species. Thus, the adsorption capacity under competitive removal conditions became highest for Cu^{2+}, followed by Pb^{2+}, Cr^{3+}, and Cd^{2+}. A calibration curve for the metal solution cannot be produced due to the presence of multiple metal species, and thus, the concentration profile could not be made for this experiment. The final concentration after CDI operation was obtained using an ICP-AES.

Figure 4.14

Conductivity and Current Profiles of the Discharge Solution from Competitive Metal Removal

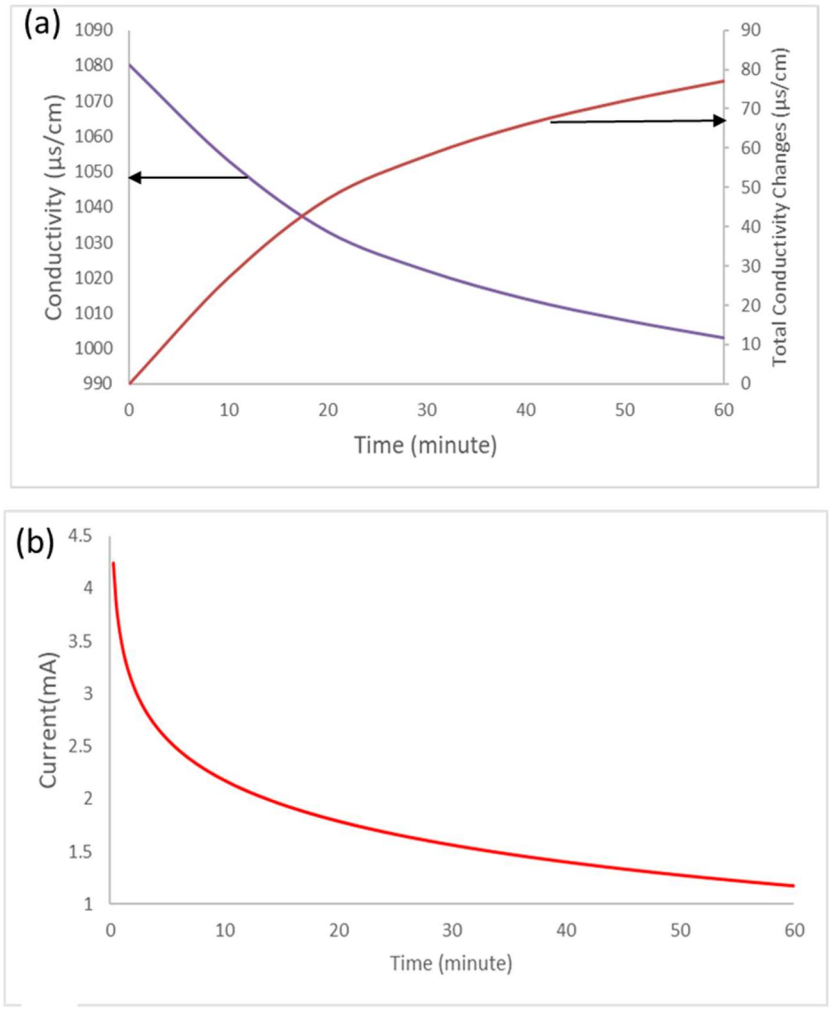

Note. These are profiles of the discharge solution during competitive metal removal operated at 1 V applied voltage, 5 ml/min flow rate with the initial concentration of 1.5 mM for each metal species within the solution.

Table 4.7
Performance Metrics of Competitive Metal Removal

Operating Conditions: AV (V), FR (mL/min)*	Metal Species	Adsorption Capacity (mg/g)	Molar Ion Adsorption Capacity (µmole/g)	Ion Adsorption Rate (mg/g·min)	Charge Efficiency
1.0 V, 5 ml/min	Chromium	2.79	11.73	0.09	0.49%
	Lead	5.26	15.88	0.05	0.66%
	Copper	3.52	18.74	0.02	0.78%
	Cadmium	1.43	6.06	0.06	0.25%
	Total	13.00	52.41	0.22	2.18%

Note. * AV = Applied Voltage, FR = Flow Rate.

The diminished ion adsorption capacities are within expectation as CDI has been known to suffer from high ion activity, in this case from the multiple metal species hampering each other adsorption. The low adsorption of Cd^{2+} in the presence of multiple species was similarly observed by (Huang et al., 2016), who provided a hypothesis that the adsorption of Cd^{2+} is outcompeted by others due to its slower adsorption mechanism, largely involving electrosorption. The largest drop in adsorption, however, was observed for Cr^{3+}, indicating that its adsorption by MnO_2/ACC electrode is greatly affected by the presence of other metal species. This decrease was not observed by (Huang et al., 2016) when working with raw activated carbon cloth, which utilized electrical double layer as an ion adsorption mechanism. Therefore, this drop in the adsorption of Cr^{3+} is due to the effect of multiple metal species on the pseudocapacitive intercalation, another adsorption mechanism utilized by the MnO_2/ACC electrode. Further investigation should be made to identify the interactions under multiple metal species conditions which hamper the adsorption process via pseudocapacitive intercalation.

For charge efficiency, the total charge efficiency reached as high as 2.18% which is second only to the individual adsorption of chromium. The high total charge efficiency can be contributed to the high ion density of the multiple metal species increasing the total ion adsorption capacity. However, since the adsorption capacity of each metal species was reduced, the actual charge efficiency for each species was much lower. Thus, it is clear that under the condition of competitive removal, the presence of multiple metal species hampers the removal of a specific metal species in both ion adsorption capacity and energy efficiency.

4.6 Heavy Metal Removal under Multiple Cycle Operation

To investigate CDI operation with the MnO_2/ACC electrode on heavy metal removal over multiple cycles, the current profiles for the removal of each metal species were recorded for 16 cycles to study their performance. The charge ratio was also calculated from these current profiles to investigate the changes in the performance and the ion adsorption. The current profiles and the charge ratio can represent the number of ions moving through the CDI system during the adsorption phase, and therefore, can be correlated to the ion adsorption performance of the CDI. The charge efficiencies in section 4.4 also support this connection in which they can be used to more accurately identify the degree to which the ion adsorption of each metal specie is proportional to their relative specific total passed charges. Therefore, the current profile and charge ratio can be used to study the changes in ion adsorption performance of the CDI for heavy metal removal over multiple cycles. As can be observed in figure 4.15 and figure 4.16, the current profiles and the charge ratio of the adsorption phase shrink over the course of multiple cycles. After 16 cycles of operation, the charge ratio of the CDI fell to 0.81, 0.84, 0.94, and 0.87 for metal removal of Cr^{3+}, Pb^{2+}, Cu^{2+}, and Cd^{2+}, respectively.

Figure 4.15

Current Profile of Multiple Cycle CDI Operation for Heavy Metal Removal of Individual Metal Species

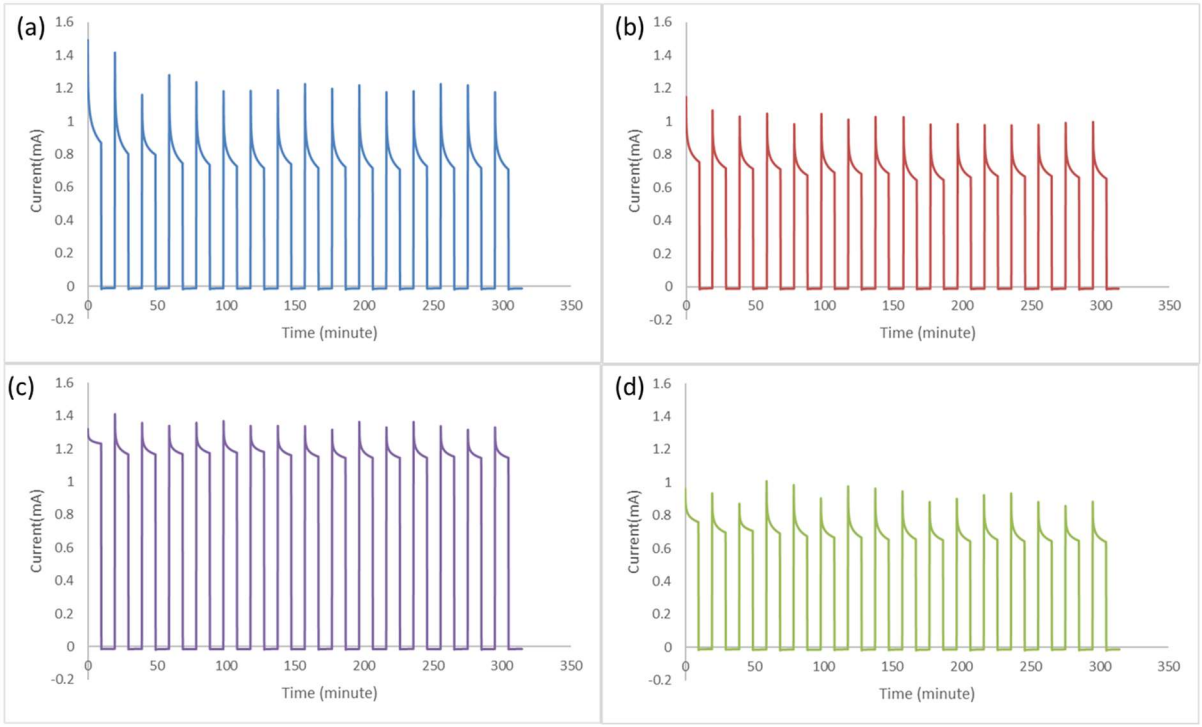

Note. Current profiles of multiple cycle CDI operation for heavy metal removal of individual metal species: (a) chromium, (b) lead, (c) copper, (d) cadmium

Figure 4.16

Current Ratio Graphs of Multiple Cycle CDI Operation for Heavy Metal Removal of Individual Metal Species

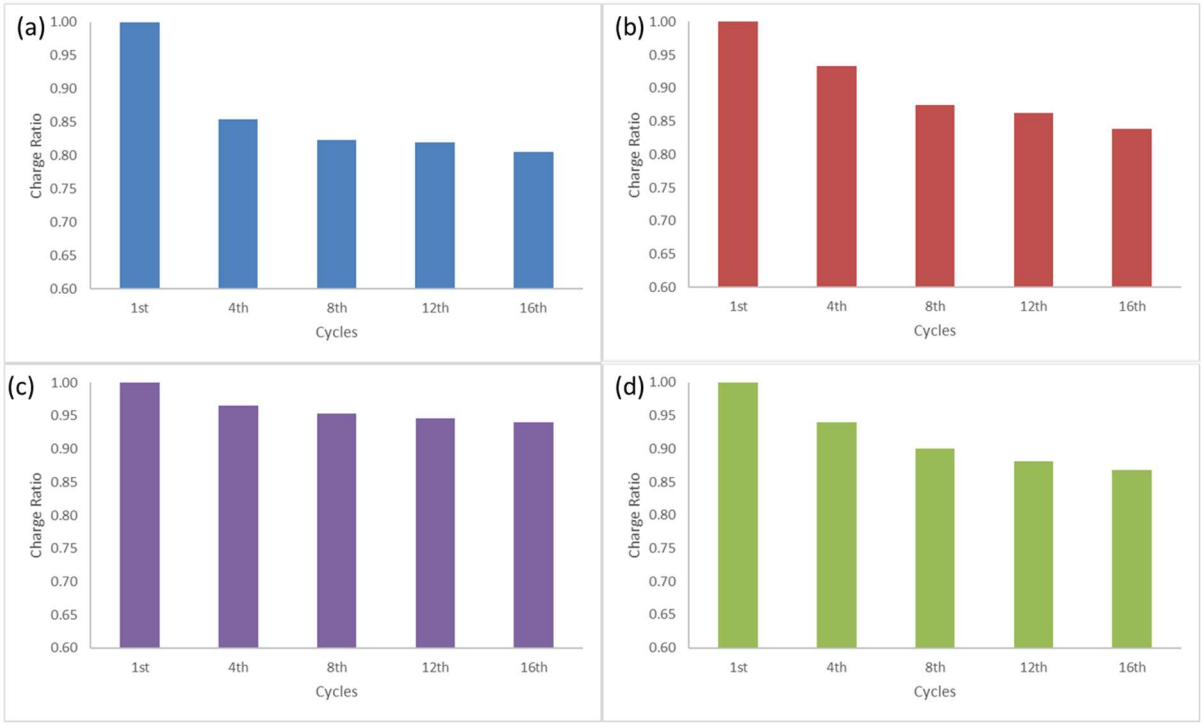

Note. Current ratio graphs of multiple cycle CDI operation for heavy metal removal of individual metal species: (a) chromium, (b) lead, (c) copper, (d) cadmium

These drops in ion adsorption of the CDI are commonly caused by changes in the ability to adsorb or desorb the ions of the electrodes. This in part can be due to slow ion desorption from the electrode caused by the complex pore system hampering the movement, or from the slow desorption of ions from the lattice structure of the deposited MnO_2. Such characteristics can be observed in the current profiles in figure 4.15 where the current profiles of the desorption phase were much smaller than the adsorption phase, suggesting slower desorption.

Without complete ion desorption from the pore structure, the adsorption capacity of the CDI would reduce over the course of multiple cycles. This explains why the adsorption of Cr^{3+} suffered the most reduction in charge ratio and adsorption performance. Since a large

amount of Cr^{3+} was adsorbed in the adsorption phase, total desorption from the electrodes was not achievable due to slow desorption, reducing the adsorption capacity and the charge ratio in the following cycles. However, this phenomenon should normally happen in an earlier cycle as an equilibrium would eventually be reached. This can be observed in figure 4.16 that the reduction in charge ratio is larger in the earlier cycle, and gradually decreases in later cycles.

However, continued reduction in charge ratio in later cycles was still observed, this is due to the redox reaction on the electrode's surface occurring from prolonged charge-discharge cycles, causing reduced active surface area and pore volume. Still, there can be other factors that can contribute to the decreasing charge ratio and ion adsorption performance. Thus, it should be investigated in future works as to what are the contributing factors in reducing the CDI performance of MnO_2 deposited electrodes over multiple cycles.

4.7 Chapter Summary

SEM and XRD results of the MnO_2/ACC samples showed successful deposition under the synthesis conditions. It is observed that deposition at a higher scan rate allowed for a more uniform spread of MnO_2 deposition, while higher deposition cycles allow for crystal growth of the MnO_2 deposits. The cyclic voltammogram showed that the MnO_2 deposition did not significantly change the electrode capacitive behavior on the voltammogram but still showed improved capacitance depending on the synthesis conditions. And in comparison, between different electrodeposition methods, cyclic voltammetry was able to produce higher areal capacitance than the amperometry method. The highest areal capacitance was achieved in samples electrodeposited at 25 mV/s scan rate and 10 cycles.

Heavy metal removal was performed on solutions of Cr^{3+}, Pb^{2+}, Cu^{2+}, and Cd^{2+}, achieving adsorption capacities of 8.76, 6.48, 3.64, and 3.41 mg/g. Effects of flow rate and cell voltage were investigated on each metal species. CDI operations with increased flow rate showed reduced ion adsorption without significant differences between each metal specie and reduced charge efficiency. CDI operations with reduced cell voltage showed reduced ion adsorption with a stronger effect on the adsorption of Cd^{2+} relative to other metal

species. A characteristic of MnO_2/ACC is observed where an increase in applied voltage reduces the charge efficiency. In competitive removal, there were diminishes in adsorption capacities and charge efficiency for all species with Cr^{3+} and Cd^{2+} showing the greatest reduction. As for operation for multiple cycles, the dropped in charge ratio after 16 cycles were largest for the adsorption of Cr^{3+} followed by Pb^{2+}, Cd^{2+}, and Cu^{2+}. This is attributed to the slow desorption of ions in the desorption phase limiting the adsorption capacity in the following adsorption phase.

CHAPTER 5
CONCLUSIONS AND FUTURE RECOMMENDATIONS

5.1 Conclusions

In this study, successful electrodeposition of MnO_2 onto activated carbon cloth using cyclic voltammetry were achieved in which the deposition conditions were also investigated. With increased deposition scan rate, MnO_2 deposits had a small structure and uniform coverage, exhibiting increased areal capacitance. With increased deposition cycles, MnO_2 deposits underwent crystal growth, forming uniform structures all over ACC fiber strands. As for the areal capacitance, an increase was observed in the higher deposition scan rate condition, while the lower deposition scan rate exhibited decreased areal capacitance instead. This is attributed to the longer deposition time allowing for increased crystal growth which blocks the pore structure of the ACC, reducing overall capacitance.

MnO_2/ACC electrodes in CDI operation had performed successful heavy metal removal, exhibiting improved adsorption capacity compared to the raw ACC. Its adsorption capacity was in descending order from chromium, lead, copper, to cadmium. The adsorption capacity has a positive correlation with the cell voltage with the largest impact on cadmium. In contrast, it has a negative correlation to the flow rate during the operation which did not differentiate between each metal specie. As for the charge efficiency, the MnO_2/ACC showed lower charge efficiency than raw ACC. The charge efficiency is inversely proportional to the flow rate and the applied voltage. MnO_2/ACC's relationship with the applied voltage is in contrast to the behavior of porous carbon and should be further investigated.

As for the competitive removal of heavy metals, the diminished adsorption of each species was observed, attributed to the high ion activity of multiple metal species. While the total charge efficiency was at a comparable level to the individual metal removal, the charge efficiency of each species under competitive conditions dropped drastically. In terms of multiple cycle operation, the current profile and the charge ratio of the CDI operation

decreased over the 16 cycles with the most drastic decrease to the removal of chromium, then lead, cadmium, and the least with copper.

5.2 Future Recommendations

MnO_2/ACC had shown successful improvement in metal removal performance, however, the deposition conditions (both scan rate and deposition cycle) should be further investigated to identify the maximum point at which the specific capacitance can be increased and the effect on the adsorption performance. BET isotherm should also be performed in future work to investigate the effect of the deposition condition on the pore structure of the electrode. And despite the successful and improved metal removal performance, the multiple cycle operation showed that its robustness still needs to be improved. Due to the variability in researching metal removal with CDI, a standard in which CDI's performance can be reliably compared and referenced should be established for future CDI research.

REFERENCES

Anderson, M. A., Cudero, A. L., & Palma, J. (2010). Capacitive deionization as an electrochemical means of saving energy and delivering clean water. Comparison to present desalination practices: Will it compete? In *Electrochimica Acta* (Vol. 55, Issue 12, pp. 3845–3856). Pergamon. https://doi.org/10.1016/j.electacta.2010.02.012

Baby, J., Raj, J., Biby, E., Sankarganesh, P., Jeevitha, M., Ajisha, S., & Rajan, S. (2011). Toxic effect of heavy metals on aquatic environment. *International Journal of Biological and Chemical Sciences*, *4*(4). https://doi.org/10.4314/ijbcs.v4i4.62976

Barakat, M. A. (2011). New trends in removing heavy metals from industrial wastewater. In *Arabian Journal of Chemistry* (Vol. 4, Issue 4, pp. 361–377). Elsevier. https://doi.org/10.1016/j.arabjc.2010.07.019

Baruth, E. E., & Bergman, R. A. (2005). Membrane Process. In *Water treatment plant design* (4th ed.). McGraw-Hill.

Baruth, E. E., & Gottlieb, M. C. (2005). ION EXCHANGE APPLICATIONS IN WATER TREATMENT. In *Water treatment plant design* (4th ed.). McGraw-Hill.

Bautista-Patacsil, L., Lazarte, J. P. L., Dipasupil, R. C., Pasco, G. Y., Eusebio, R. C., Orbecido, A., & Doong, R. (2020). Deionization utilizing reduced graphene oxide-titanium dioxide nanotubes composite for the removal of Pb^{2+} and Cu^{2+}. *Journal of Environmental Chemical Engineering*, *8*(3), 103063. https://doi.org/10.1016/j.jece.2019.103063

Bharath, G., Alhseinat, E., Ponpandian, N., Khan, M. A., Siddiqui, M. R., Ahmed, F., & Alsharaeh, E. H. (2017). Development of adsorption and electrosorption techniques for removal of organic and inorganic pollutants from wastewater using novel magnetite/porous graphene-based nanocomposites. *Separation and Purification Technology*, *188*, 206–218. https://doi.org/10.1016/j.seppur.2017.07.024

Boretti, A., & Rosa, L. (2019). Reassessing the projections of the World Water Development Report. *Npj Clean Water*, *2*(1), 1–6. https://doi.org/10.1038/s41545-019-0039-9

Broughton, J. N., & Brett, M. J. (2005). Variations in MnO_2 electrodeposition for electrochemical capacitors. *Electrochimica Acta*, *50*(24), 4814–4819. https://doi.org/10.1016/J.ELECTACTA.2005.03.006

Byles, B. W., Cullen, D. A., More, K. L., & Pomerantseva, E. (2018). Tunnel structured manganese oxide nanowires as redox active electrodes for hybrid capacitive deionization. *Nano Energy*, *44*, 476–488. https://doi.org/10.1016/J.NANOEN.2017.12.015

Byles, B. W., Hayes-Oberst, B., & Pomerantseva, E. (2018). Ion Removal Performance, Structural/Compositional Dynamics, and Electrochemical Stability of Layered Manganese Oxide Electrodes in Hybrid Capacitive Deionization. *ACS Applied Materials & Interfaces*, *10*(38), 32313–32322. https://doi.org/10.1021/ACSAMI.8B09638

Carolin, C. F., Kumar, P. S., Saravanan, A., Joshiba, G. J., & Naushad, M. (2017). Efficient techniques for the removal of toxic heavy metals from aquatic environment: A review. In *Journal of Environmental Chemical Engineering* (Vol. 5, Issue 3, pp. 2782–2799). Elsevier Ltd. https://doi.org/10.1016/j.jece.2017.05.029

Chaiyara, R., Ngoendee, M., & Kruatrachue, M. (2013). Accumulation of Cd, Cu, Pb, and Zn in water, sediments, and mangrove crabs (Sesarma mederi) in the upper Gulf of Thailand. *ScienceAsia*, *39*(4), 376–383. https://doi.org/10.2306/scienceasia1513-1874.2013.39.376

Chang, J. K., Chen, Y. L., & Tsai, W. T. (2004). Effect of heat treatment on material characteristics and pseudo-capacitive properties of manganese oxide prepared by anodic deposition. *Journal of Power Sources*, *135*(1–2), 344–353. https://doi.org/10.1016/J.JPOWSOUR.2004.03.076

Chen, R., Sheehan, T., Ng, J. L., Brucks, M., & Su, X. (2020). Capacitive deionization and electrosorption for heavy metal removal. In *Environmental Science: Water Research and Technology* (Vol. 6, Issue 2, pp. 258–282). Royal Society of Chemistry. https://doi.org/10.1039/c9ew00945k

Chen, Y., Peng, L., Zeng, Q., Yang, Y., Lei, M., Song, H., Chai, L., & Gu, J. (2015). Removal of trace Cd(II) from water with the manganese oxides/ACF composite

electrode. *Clean Technologies and Environmental Policy*, *17*(1), 49–57. https://doi.org/10.1007/s10098-014-0756-1

Choi, J., Dorji, P., Shon, H. K., & Hong, S. (2019). Applications of capacitive deionization: Desalination, softening, selective removal, and energy efficiency. In *Desalination* (Vol. 449, pp. 118–130). Elsevier B.V. https://doi.org/10.1016/j.desal.2018.10.013

Cohen, I., Avraham, E., Bouhadana, Y., Soffer, A., & Aurbach, D. (2013). Long term stability of capacitive de-ionization processes for water desalination: The challenge of positive electrodes corrosion. *Electrochimica Acta*, *106*, 91–100. https://doi.org/10.1016/j.electacta.2013.05.029

Dupont, M. F., & Donne, S. W. (2014). Nucleation and Growth of Electrodeposited Manganese Dioxide for Electrochemical Capacitors. *Electrochimica Acta*, *120*, 219–225. https://doi.org/10.1016/j.electacta.2013.12.014

Edelstein, M., & Ben-Hur, M. (2018). Heavy metals and metalloids: Sources, risks and strategies to reduce their accumulation in horticultural crops. In *Scientia Horticulturae* (Vol. 234, pp. 431–444). Elsevier B.V. https://doi.org/10.1016/j.scienta.2017.12.039

Elisadiki, J., & King'ondu, C. K. (2020). Performance of ion intercalation materials in capacitive deionization/electrochemical deionization: A review. In *Journal of Electroanalytical Chemistry* (Vol. 878, p. 114588). Elsevier B.V. https://doi.org/10.1016/j.jelechem.2020.114588

Fu, F., & Wang, Q. (2011). Removal of heavy metal ions from wastewaters: A review. In *Journal of Environmental Management* (Vol. 92, Issue 3, pp. 407–418). Academic Press. https://doi.org/10.1016/j.jenvman.2010.11.011

Gaikwad, M. S., & Balomajumder, C. (2017). Tea waste biomass activated carbon electrode for simultaneous removal of Cr(VI) and fluoride by capacitive deionization. *Chemosphere*, *184*, 1141–1149. https://doi.org/10.1016/j.chemosphere.2017.06.074

Han, B., Cheng, G., Wang, Y., & Wang, X. (2019). Structure and functionality design of novel carbon and faradaic electrode materials for high-performance capacitive deionization. In *Chemical Engineering Journal* (Vol. 360, pp. 364–384). Elsevier

B.V. https://doi.org/10.1016/j.cej.2018.11.236

Hu, C. C., & Tsou, T. W. (2002). Capacitive and textural characteristics of hydrous manganese oxide prepared by anodic deposition. *Electrochimica Acta*, *47*(21), 3523–3532. https://doi.org/10.1016/S0013-4686(02)00321-3

Hu, C., Liu, F., Lan, H., Liu, H., & Qu, J. (2015). Preparation of a manganese dioxide/carbon fiber electrode for electrosorptive removal of copper ions from water. *Journal of Colloid and Interface Science*, *446*, 380–386. https://doi.org/10.1016/j.jcis.2014.12.051

Huang, C.-C., & Su, Y.-J. (2010). Removal of copper ions from wastewater by adsorption/electrosorption on modified activated carbon cloths. *Journal of Hazardous Materials*, *175*(1–3), 477–483. https://doi.org/10.1016/j.jhazmat.2009.10.030

Huang, Z., Lu, L., Cai, Z., & Ren, Z. J. (2016). Individual and competitive removal of heavy metals using capacitive deionization. *Journal of Hazardous Materials*, *302*, 323–331. https://doi.org/10.1016/J.JHAZMAT.2015.09.064

Jain, C. K., Singhal, D. C., & Sharma, M. K. (2005). Metal Pollution Assessment of Sediment and Water in the River Hindon, India. *Environmental Monitoring and Assessment*, *105*(1–3), 193–207. https://doi.org/10.1007/s10661-005-3498-z

Kalfa, A., Shapira, B., Shopin, A., Cohen, I., Avraham, E., & Aurbach, D. (2020). Capacitive deionization for wastewater treatment: Opportunities and challenges. In *Chemosphere* (Vol. 241, p. 125003). Elsevier Ltd. https://doi.org/10.1016/j.chemosphere.2019.125003

Kiatsayomphu, S., & Chaiklieng, S. (2012). □□□ Assessment on Heavy Metals Contamination and Health Risk of Contaminant Exposure from Consumptions of Fish in Loeng Puay Marsh at Khon Kaen Province□. In *Thai J Toxicology* (Vol. 26, Issue 2). https://li01.tci-thaijo.org/index.php/ThaiJToxicol/article/view/244053

Kurniawan, T. A., Chan, G. Y. S., Lo, W. H., & Babel, S. (2006). Physico-chemical treatment techniques for wastewater laden with heavy metals. *Chemical Engineering Journal*, *118*(1–2), 83–98. https://doi.org/10.1016/j.cej.2006.01.015

Lee, B. J., Sivakkumar, S. R., Ko, J. M., Kim, J. H., Jo, S. M., & Kim, D. Y. (2007).

Carbon nanofibre/hydrous RuO2 nanocomposite electrodes for supercapacitors. *Journal of Power Sources*, *168*(2), 546–552. https://doi.org/10.1016/j.jpowsour.2007.02.076

Lee, J.-H. H.-J. D. J.-I. Y.-J. H.-J. (2015). Effect of surface modification of carbon felts on capacitive deionization for desalination. *Carbon Letters*, *16*(2), 93–100. https://doi.org/10.5714/CL.2015.16.2.093

Li, M., & Park, H. G. (2018). Pseudocapacitive Coating for Effective Capacitive Deionization. *ACS Applied Materials and Interfaces*, *10*(3), 2442–2450. https://doi.org/10.1021/acsami.7b14643

Lin, S. C., Lu, Y. T., Chien, Y. A., Wang, J. A., Chen, P. Y., Ma, C. C. M., & Hu, C. C. (2018). Asymmetric supercapacitors based on electrospun carbon nanofiber/sodium-pre-intercalated manganese oxide electrodes with high power and energy densities. *Journal of Power Sources*, *393*, 1–10. https://doi.org/10.1016/j.jpowsour.2018.05.019

Liu, P., Yan, T., Zhang, J., Shi, L., & Zhang, D. (2017). Separation and recovery of heavy metal ions and salt ions from wastewater by 3D graphene-based asymmetric electrodes via capacitive deionization. *Journal of Materials Chemistry A*, *5*(28), 14748–14757. https://doi.org/10.1039/C7TA03515B

Liu, Y.-X., Yuan, D.-X., Yan, J.-M., Li, Q.-L., & Ouyang, T. (2011). Electrochemical removal of chromium from aqueous solutions using electrodes of stainless steel nets coated with single wall carbon nanotubes. *Journal of Hazardous Materials*, *186*(1), 473–480. https://doi.org/10.1016/j.jhazmat.2010.11.025

Liu, Y., Yan, J., Yuan, D., Li, Q., & Wu, X. (2013). The study of lead removal from aqueous solution using an electrochemical method with a stainless steel net electrode coated with single wall carbon nanotubes. *Chemical Engineering Journal*, *218*, 81–88. https://doi.org/10.1016/j.cej.2012.12.020

Phenrat, T., Otwong, A., Chantharit, A., & Lowry, G. V. (2016). Ten-year monitored natural recovery of lead-contaminated mine tailing in Klity Creek, Kanchanaburi Province, Thailand. In *Environmental Health Perspectives* (Vol. 124, Issue 10, pp. 1511–1520). Public Health Services, US Dept of Health and Human Services. https://doi.org/10.1289/EHP215

Polprasert, C. (1982). Heavy metal pollution in the Chao Phraya River estuary, Thailand. *Water Research*, *16*(6), 775–784. https://doi.org/10.1016/0043-1354(82)90004-5

Porada, S., Zhao, R., Van Der Wal, A., Presser, V., & Biesheuvel, P. M. (2013). Review on the science and technology of water desalination by capacitive deionization. In *Progress in Materials Science* (Vol. 58, Issue 8, pp. 1388–1442). Elsevier Ltd. https://doi.org/10.1016/j.pmatsci.2013.03.005

Prasad, K. R., & Miura, N. (2004). Potentiodynamically deposited nanostructured manganese dioxide as electrode material for electrochemical redox supercapacitors. *Journal of Power Sources*, *135*(1–2), 354–360. https://doi.org/10.1016/J.JPOWSOUR.2004.04.005

Qiao, S., Shi, X., Fang, X., Liu, S., Kornkanitnan, N., Gao, J., Zhu, A., Hu, L., & Yu, Y. (2015). Heavy metal and clay mineral analyses in the sediments of Upper Gulf of Thailand and their implications on sedimentary provenance and dispersion pattern. *Journal of Asian Earth Sciences*, *114*, 488–496. https://doi.org/10.1016/j.jseaes.2015.04.043

Rana-Madaria, P., Nagarajan, M., Rajagopal, C., & Garg, B. S. (2005). Removal of Chromium from Aqueous Solutions by Treatment with Carbon Aerogel Electrodes Using Response Surface Methodology. *Industrial & Engineering Chemistry Research*, *44*(17), 6549–6559. https://doi.org/10.1021/ie050321p

Shi, W., Zhou, X., Li, J., Meshot, E. R., Taylor, A. D., Hu, S., Kim, J.-H., Elimelech, M., & Plata, D. L. (2018). High-Performance Capacitive Deionization via Manganese Oxide-Coated, Vertically Aligned Carbon Nanotubes. *Environmental Science & Technology Letters*, *5*(11), 692–700. https://doi.org/10.1021/ACS.ESTLETT.8B00397

Shinomiya, T., Gupta, V., & Miura, N. (2006). Effects of electrochemical-deposition method and microstructure on the capacitive characteristics of nano-sized manganese oxide. *Electrochimica Acta*, *51*(21), 4412–4419. https://doi.org/10.1016/J.ELECTACTA.2005.12.025

Sow, A. Y., Dee, K. H., Lee, S. W., & Eh Rak, A. A. L. (2019). An assessment of heavy metals toxicity in Asian Clam, Corbicula fluminea, from Mekong River, Pa Sak River, and Lopburi River, Thailand. *Scientific World Journal*, *2019*.

https://doi.org/10.1155/2019/1615298

Suss, M. E., & Presser, V. (2018). Water Desalination with Energy Storage Electrode Materials. In *Joule* (Vol. 2, Issue 1, pp. 10–15). Cell Press. https://doi.org/10.1016/j.joule.2017.12.010

Tan, G., Lu, S., Xu, N., Gao, D., & Zhu, X. (2020). Pseudocapacitive Behaviors of Polypyrrole Grafted Activated Carbon and MnO_2 Electrodes to Enable Fast and Efficient Membrane-Free Capacitive Deionization. *Environmental Science and Technology*, *54*(9), 5843–5852. https://doi.org/10.1021/acs.est.9b07182

Thamilselvan, A., Nesaraj, A. S., Noel, M., & James, E. J. (2015). Effect of Chemically Treated / Untreated Carbon Cloth: Potential Use as Electrode Materials in the Capacitive Deionization Process of Desalination of Aqueous Salt Solution. *Journal of Electrochemical Science and Technology*, *6*(4), 139–145. https://doi.org/10.5229/JECST.2015.6.4.139

Tortajada, C., & Fernandez, V. (2018). Towards global water security: A departure from the status quo? In *Water Resources Development and Management* (pp. 1–19). Springer. https://doi.org/10.1007/978-981-10-7913-9_1

Vardhan, K. H., Kumar, P. S., & Panda, R. C. (2019). A review on heavy metal pollution, toxicity and remedial measures: Current trends and future perspectives. In *Journal of Molecular Liquids* (Vol. 290, p. 111197). Elsevier B.V. https://doi.org/10.1016/j.molliq.2019.111197

Wang, H., & Na, C. (2014). Binder-Free Carbon Nanotube Electrode for Electrochemical Removal of Chromium. *ACS Applied Materials & Interfaces*, *6*(22), 20309–20316. https://doi.org/10.1021/am505838r

Wang, Y., & Fang, P. (2016). *Analysis of the impact of heavy metal on the Chinese aquaculture and the ecological hazard*. 42–47. https://doi.org/10.2991/ifeesd-16.2016.8

Wongsasuluk, P., Chotpantarat, S., Siriwong, W., & Robson, M. (2014). Heavy metal contamination and human health risk assessment in drinking water from shallow groundwater wells in an agricultural area in Ubon Ratchathani province, Thailand. *Environmental Geochemistry and Health*, *36*(1), 169–182. https://doi.org/10.1007/s10653-013-9537-8

Wu, T., Wang, G., Wang, S., Zhan, F., Fu, Y., Qiao, H., & Qiu, J. (2018). Highly Stable Hybrid Capacitive Deionization with a MnO_2 Anode and a Positively Charged Cathode. *Environmental Science and Technology Letters*, *5*(2), 98–102. https://doi.org/10.1021/acs.estlett.7b00540

Yin, S., Feng, C., Li, Y., Yin, L., & Shen, Z. (2015). Heavy metal pollution in the surface water of the Yangtze Estuary: A 5-year follow-up study. *Chemosphere*, *138*, 718–725. https://doi.org/10.1016/j.chemosphere.2015.07.060

Yu, R., He, L., Cai, R., Li, B., Li, Z., & Yang, K. (2017). Heavy metal pollution and health risk in China. *Global Health Journal*, *1*(1), 47–55. https://doi.org/10.1016/s2414-6447(19)30059-4

Zafar Marg, B., & Delhi, N. (2011). *HAZARDOUS METALS AND MINERALS POLLUTION IN INDIA: SOURCES, TOXICITY AND MANAGEMENT Indian National Science Academy*.

Zhang, X. F., Wang, B., Yu, J., Wu, X. N., Zang, Y. H., Gao, H. C., Su, P. C., & Hao, S. Q. (2018). Three-dimensional honeycomb-like porous carbon derived from corncob for the removal of heavy metals from water by capacitive deionization. *RSC Advances*, *8*(3), 1159–1167. https://doi.org/10.1039/C7RA10689K

Zhang, Yanping, Sun, X., Pan, L., Li, H., Sun, Z., Sun, C., & Tay, B. K. (2009). Carbon nanotube-ZnO nanocomposite electrodes for supercapacitors. *Solid State Ionics*, *180*(32–35), 1525–1528. https://doi.org/10.1016/j.ssi.2009.10.001

Zhang, Yujie, Xue, Q., Li, F., & Dai, J. (2019). Removal of heavy metal ions from wastewater by capacitive deionization using polypyrrole/chitosan composite electrode. *Adsorption Science & Technology*, *37*(3–4), 205–216. https://doi.org/10.1177/0263617418822225

Zhao, C., Lv, X., Li, J., Xie, T., Qi, Y., & Chen, W. (2017). Manganese Oxide Nanoparticles Decorated Ordered Mesoporous Carbon Electrode for Capacitive Deionization of Brackish Water. *Journal of The Electrochemical Society*, *164*(13), E505–E511. https://doi.org/10.1149/2.0141714jes

Zhao, R., Biesheuvel, P. M., Miedema, H., Bruning, H., & van der Wal, A. (2010). Charge Efficiency: A Functional Tool to Probe the Double-Layer Structure Inside of Porous Electrodes and Application in the Modeling of Capacitive Deionization.

The Journal of Physical Chemistry Letters, *1*(1), 205–210. https://doi.org/10.1021/jz900154h

Zhao, X., Wei, H., Zhao, H., Wang, Y., & Tang, N. (2020). Electrode materials for capacitive deionization: A review. In *Journal of Electroanalytical Chemistry* (Vol. 873, p. 114416). Elsevier B.V. https://doi.org/10.1016/j.jelechem.2020.114416

Ziati, M., & Hazourli, S. (2019). Experimental investigation of activated carbon prepared from date stones adsorbent electrode for electrosorption of lead from aqueous solution. *Microchemical Journal*, *146*, 164–169. https://doi.org/10.1016/j.microc.2018.12.041

Ziati, M., Khemmari, F., Kecir, M., & Hazourli, S. (2017). Removal of chromium from tannery wastewater by electrosorption on carbon prepared from peach stones: effect of applied potential. *Carbon Letters*, *21*, 81–85. https://doi.org/10.5714/CL.2017.21.081

APPENDIX

APPENDIX A

Capacitive Deionization Setup

Following are pictures of the capacitive deionization cell and system setup.

Figure A1 Capacitive Deionization Cell

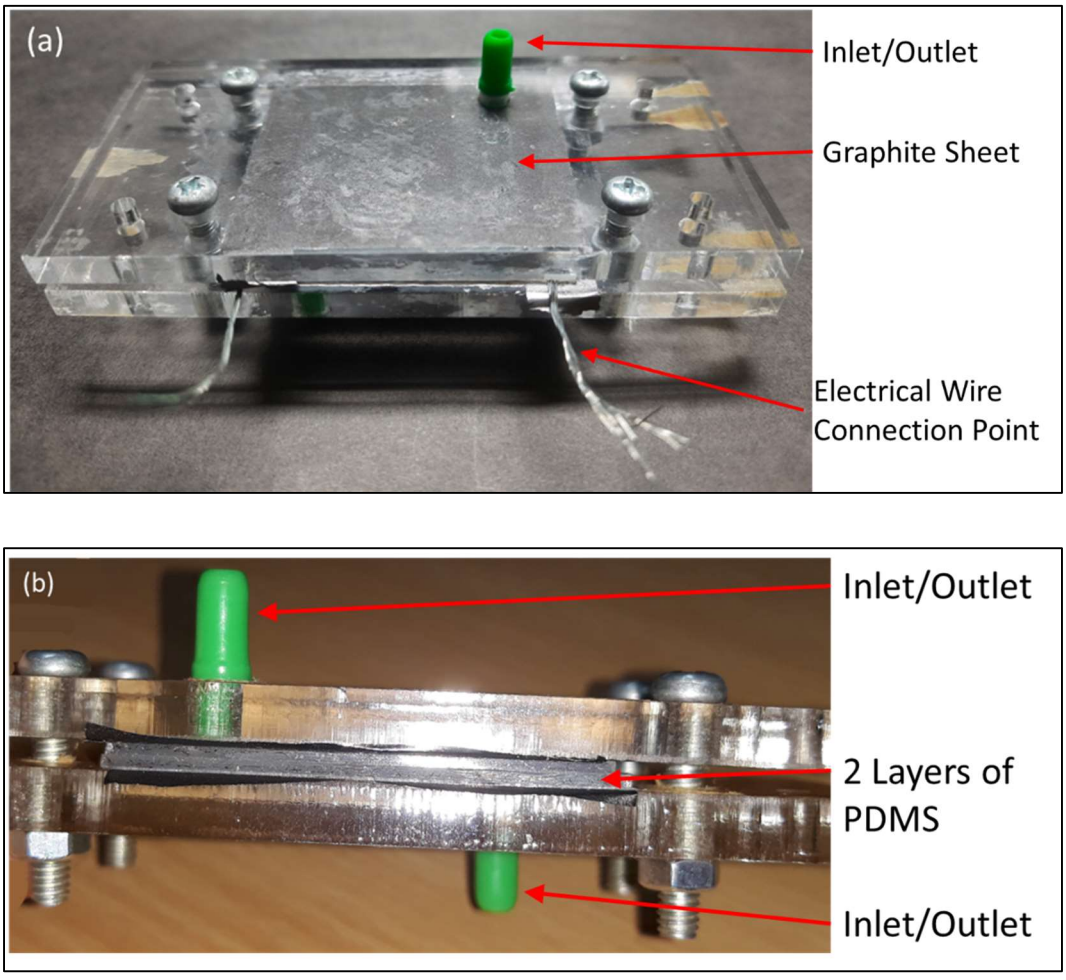

Note. Figures of the capacitive deionization cell from (a) above and from (b) the side.

Figure A2 Capacitive Deionization System Setup

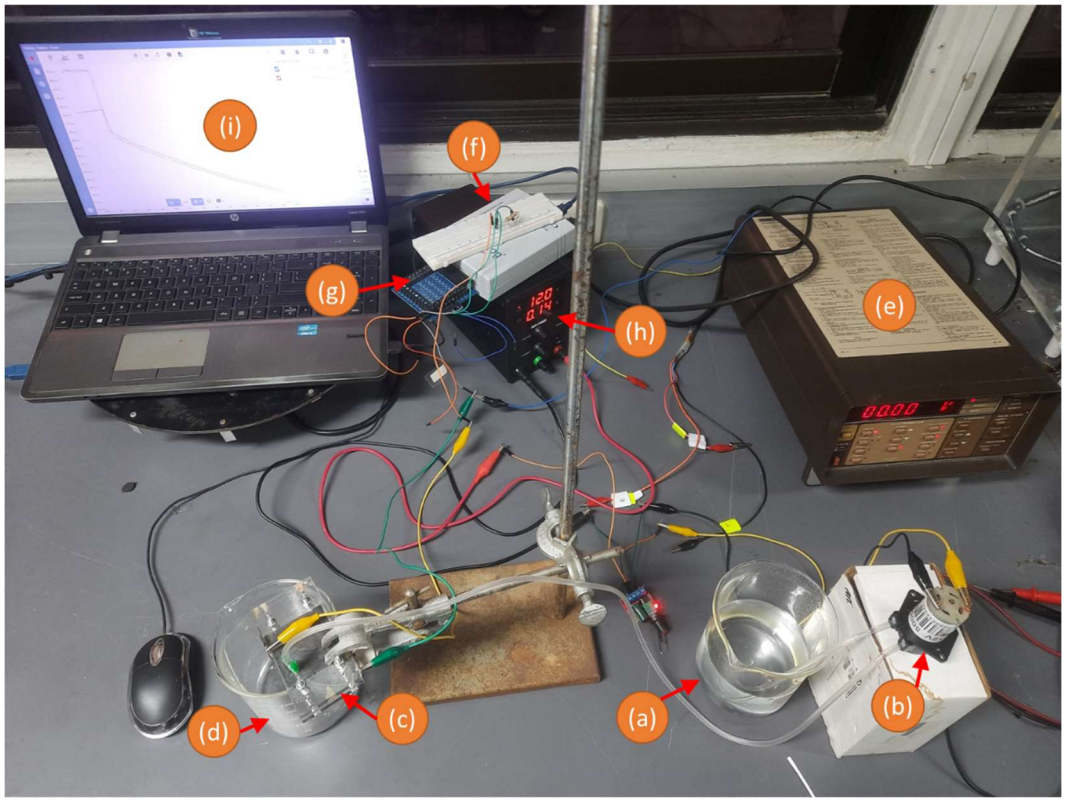

Note. Figures of the capacitive deionization system setup: (a) solution tank, (b) peristaltic pump, (c) CDI cell, (d) Reservoir, (e) Power supply, (f) resistance circuit, (g) data logger, (h) peristaltic pump's power supply, and (i) PicoLog program for data recording.